Conformational Interconversion of the *trans*-4-Hydroxynonenal-Derived (6*S*,8*R*,11*S*) 1,N^2-Deoxyguanosine Adduct When Mismatched with Deoxyadenosine in DNA

Hai Huang,[†] Hao Wang,[†] R. Stephen Lloyd,[‡] Carmelo J. Rizzo,[†] and Michael P. Stone*,[†]

Department of Chemistry, Center in Molecular Toxicology, Center for Structural Biology and Vanderbilt-Ingram Cancer Center, Vanderbilt University, Nashville, Tennessee 37235, and Center for Research in Occupational and Environmental Toxicology, Oregon Health and Science University, 3181 SW Sam Jackson Park Road, L606, Portland, Oregon 97239-3098

Received August 26, 2008

The (6*S*,8*R*,11*S*) 1,N^2-HNE-dGuo adduct of *trans*-4-hydroxynonenal (HNE) was incorporated into the duplex 5′-d(GCTAGCXAGTCC)-3′•5′-d(GGACTAGCTAGC)-3′ [X = (6*S*,8*R*,11*S*) HNE-dG], in which the lesion was mismatched opposite dAdo. The (6*S*,8*R*,11*S*) adduct maintained the ring-closed 1,N^2-HNE-dG structure. This was in contrast to when this adduct was correctly paired with dCyd, conditions under which it underwent ring opening and rearrangement to diastereomeric minor groove cyclic hemiacetals [Huang, H., Wang, H., Qi, N., Lloyd, R. S., Harris, T. M., Rizzo, C. J., and Stone, M. P. (2008) *J. Am. Chem. Soc. 130*, 10898−10906]. The (6*S*,8*R*,11*S*) adduct exhibited a *syn*/*anti* conformational equilibrium about the glycosyl bond. The *syn* conformation was predominant in acidic solution. Structural analysis of the *syn* conformation revealed that X^7 formed a distorted base pair with the complementary protonated A^{18}. The HNE moiety was located in the major groove. Structural perturbations were observed at the neighbor C^6•G^{19} and A^8•T^{17} base pairs. At basic pH, the *anti* conformation of X^7 was the major species. The 1,N^2-HNE-dG intercalated and displaced the complementary A^{18} in the 5′-direction, resulting in a bulge at the X^7•A^{18} base pair. The HNE aliphatic chain was oriented toward the minor groove. The Watson−Crick hydrogen bonding of the neighboring A^8•T^{17} base pair was also disrupted.

Introduction

trans-4-Hydroxynonenal (HNE)[1] is produced from the metabolism of membrane lipids (*1*), and it is the major in vivo peroxidation product of ω-6 polyunsaturated fatty acids (*2, 3*). Several routes for the formation of HNE from ω-6 polyunsaturated fatty acids have been described (*4*−*6*). HNE forms Michael addition adducts with protein Cys, His, and Lys residues, which can further rearrange to cyclic hemiacetals (*2, 7*−*11*). Many of the cytotoxic effects attributed to HNE involve alteration in gene expression and cell signaling to cell proliferation and apoptosis (*12*−*18*), and these are associated with the etiology of human disease arising as a result of oxidative stress, for example, Alzheimer's disease (*19*), Parkinson's disease (*20*), arteriosclerosis (*21*), and hepatic ischemia reperfusion injury (*22*).

Michael addition of the N^2-amino group of dGuo to HNE gives four diastereomeric HNE-derived 1,N^2-dGuo (1,N^2-HNE-dGuo) adducts (Figure 1) (*23*−*26*), which have been detected in cellular DNA (*27*−*33*). Wang et al. (*34, 35*) synthesized the four stereoisomers of the exocyclic 1,N^2-HNEdGuo dG adduct and incorporated them into 5′-d(GCTAGCXAGTCC)-3′•5′-d(GGACTCGCTAGC)-3′, in which X denotes the 1,N^2-HNE-dGuo adduct. When placed opposite dCyd in duplex DNA, the exocyclic 1,N^2-HNE-dGuo adducts underwent ring opening at the N1 imine nitrogen of dGuo, thus exposing the Watson−Crick base pairing face of the adducted dG. The diastereomeric (6*S*,8*R*,11*S*) and (6*R*,8*S*,11*R*) 1,N^2-HNE-dGuo adducts in fact existed primarily as minor groove cyclic hemiacetals when placed into this duplex (Scheme 1) (*36*). The initial ring opening of the 1,N^2-HNE-dGuo adducts likely occurs via a mechanism similar to that proposed for the related 3-(2′-deoxy-β-D-*erythro*-pentofuranosyl)pyrimido[1,2-α]purin-10(3*H*)-one (M_1dG) adduct (*37, 38*). It should also be noted that an alternative pathway to the formation of HNE-derived DNA adducts involves oxidation of HNE to 2,3-epoxy-4-hydroxynonanal, yielding etheno adducts (*39*−*43*).

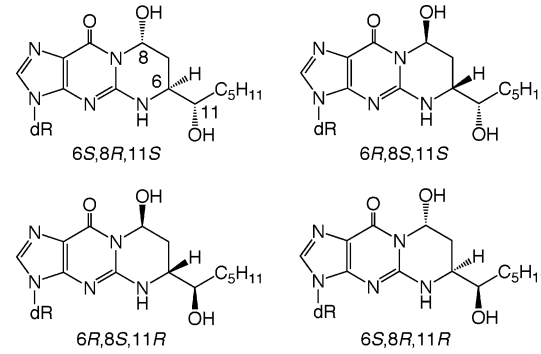

Figure 1. Four stereoisomers of HNE-derived exocyclic 1,N^2-deoxyguanosine adducts.

The potential to form DNA adducts (Figure 1) suggests that HNE may be genotoxic. HNE induces the SOS response in *Escherichia coli* (*44*). Chromosomal aberrations are observed

* To whom correspondence should be addressed. Tel: 615-322-2589. Fax: 615-322-7591. E-mail: michael.p.stone@vanderbilt.edu.
[†] Vanderbilt University.
[‡] Oregon Health and Science University.

[1] Abbreviations: HNE, *trans*-4-hydroxynonenal; 1,N^2-HNE-dG, HNE derived 1,N^2-2′-deoxyguanosine adduct; PdG, 1,N^2-propano-2′-deoxyguanosine; M_1dG, 3-(2′-deoxy-β-D-*erythro*-pentofuranosyl)pyrimido[1,2-α]purin-10(3*H*)-one; NOESY, nuclear Overhauser effect spectroscopy; COSY, correlation spectroscopy; TOCSY, total correlation spectroscopy; DQF-COSY, double-quantum filtered COSY; NOE, nuclear Overhauser effect; rMD, restrained molecular dynamics.

10.1021/tx800320m CCC: $40.75
Published on Web 12/03/2008

Scheme 1. Ring Chain Tautomerization of HNE-Derived Diastereomeric (6*S*,8*R*,11*S*) 1,N^2-dGuo Adduct When Placed Opposite dCyd

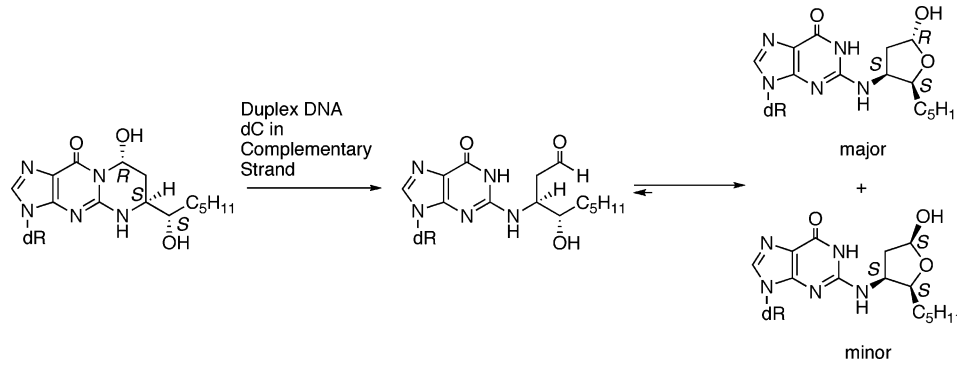

upon exposures to HNE in rodent (*45, 46*), mammalian (*47, 48*), and human (*49*) cells. In mammalian cells, the genotoxicity of HNE depends upon glutathione levels, which modulate the formation of HNE-DNA adducts (*50*−*52*). The mutational spectrum induced by HNE adducts in the *lacZ* gene of the single-stranded M13 phage transfected into wild-type *E. coli* revealed recombination events, C→T transitions, followed by G→C and A→C transversions, and frameshift mutations (*25*). HNE is mutagenic (*53*) and carcinogenic in rodent cells (*54*). Hussain et al. (*55*) reported that HNE caused G→T transversions at codon 249 of wild-type *p53* in lymphosblastoid cells. Hu et al. (*56*) reported that HNE-DNA adducts were preferentially formed with guanine at the third base of codon 249 in the *p53* gene. The mutational spectrum induced by HNE adducts in the *supF* gene of shuttle vector pSP189 replicated in human cells showed that HNE induced primarily G→T transversions, accompanied by lower levels of G→A transitions (*57*). Fernandes et al. (*58*) conducted site-specific mutagenesis studies and observed that the (6*S*,8*R*,11*S*) and (6*R*,8*S*,11*R*) 1,N^2-HNE-dGuo adducts were mutagenic, inducing low levels of G→T transversions and G→A transitions. The nucleotide excision repair pathway is involved in the excision of HNE-dG lesions (*57, 59, 60*).

The propensity of the 1,N^2-HNE-dGuo adducts to undergo ring opening when placed opposite dCyd in duplex DNA, potentially facilitating successful lesion bypass by Y-family polymerases, may account for the low levels of mutations associated with these lesions (*58*). Wolfle et al. (*61*) reported that the sequential activity of pols ι and κ bypassed the (6*S*,8*R*,11*S*) and (6*R*,8*S*,11*R*) 1,N^2-HNE-dGuo adducts. Significantly, pol ι correctly inserted dCTP and to a lesser extent dTTP opposite the HNE adduct. Further extension was achieved in the presence of pol κ, which elongated from a dCyd: 1,N^2-HNE-dGuo template primer terminus (*61*).

In the present work, the (6*S*,8*R*,11*S*) 1,N^2-HNE-dGuo adduct (*36*) has been examined as to structure in 5′-d(GCTAGCX-AGTCC)-3′•5′-d(GGACTAGCTAGC)-3′, containing the X•dAdo mismatched sequence [X = (6*S*,8*R*,11*S*) 1,N^2-HNE-dGuo], using NMR (Scheme 2). This duplex mimics the situation following incorrect incorporation of dATP opposite the (6*S*,8*R*,11*S*) 1,N^2-HNE-dGuo adduct and leading to HNE-induced G→T transversions (*55, 57, 58*). Solution structures of the oligodeoxynucleotide duplex have been refined from NMR data collected as a function of pH. The (6*S*,8*R*,11*S*) 1,N^2-HNE-dGuo adduct maintains the exocyclic structure when placed complementary to dAdo. The adduct undergoes a *syn*/*anti* conformational equilibrium about the glycosyl bond, as was predicted by Xing et al. (*26*). The *syn* conformation predominates in acidic solution. Structural analysis reveals that X^7 forms a distorted base pair

Scheme 2. (A) Numbering Scheme of the Mismatched 5′-CpX-3′ Duplex and (B) Numbering Scheme of the Stereospecific HNE-Derived 1,N^2-dGuo Adduct

A

5′-G^1 C^2 T^3 A^4 G^5 C^6 X^7 A^8 G^9 $T^{10}C^{11}C^{12}$-3′
3′-$C^{24}G^{23}A^{22}T^{21}C^{20}G^{19}A^{18}T^{17}C^{16}A^{15}G^{14}G^{13}$-5′

B

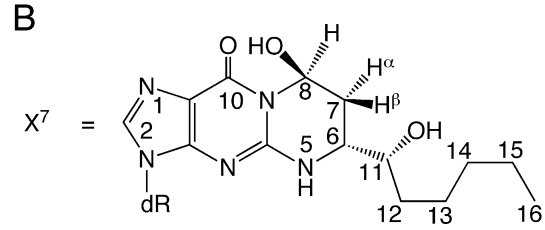

with the complementary protonated A^{18}. The HNE moiety is located in the major groove. Structural perturbations are observed at the neighbor C^6•G^{19} and A^8•T^{17} base pairs. At basic pH, the *anti* conformation of X^7 is the major species. The 1,N^2-HNE-dGuo intercalates and displaces the complementary A^{18} in the 5′-direction, resulting in a bulge at the X^7•A^{18} base pair. The HNE aliphatic chain is oriented toward the minor groove. The Watson−Crick hydrogen bonding of the neighboring A^8•T^{17} base pair is also disrupted.

Materials and Methods

Materials. The oligodeoxynucleotide 5′-d(GGACTAGC-TAGC)-3′ was synthesized and purified by anion-exchange chromatography by the Midland Certified Reagent Co. (Midland, TX). The 1,N^2-HNE-dGuo adduct of (6*S*,8*R*,11*S*) configuration was incorporated into 5′-d(GCTAGCXAGTCC)-3′ [X = (6*S*,8*R*,11*S*) 1,N^2-HNE-dGuo] as reported (*34, 35*). The oligodeoxynucleotides were characterized by MALDI-TOF mass spectrometry. Capillary gel electrophoresis and C-18 HPLC were utilized to assess their purities. The oligodeoxynucleotides were desalted by chromatography on Sephadex G-25 (Sigma-Aldrich, St. Louis, MO). Oligodeoxynucleotide concentrations were determined by UV absorption at 260 nm, using calculated extinction coefficients for both sequences of 1.1×10^5 L mol^{-1} cm^{-1} (*62*). The strands were annealed at 1:1 stoichiometry in 10 mM NaH_2PO_4, 100 mM NaCl, and 50 μM Na_2EDTA (pH 7.0). The solutions were heated to 95 °C for 10 min and cooled to room temperature. The duplex DNA was purified using DNA grade hydroxylapatite chromatography, with a gradient from 10 to 200 mM NaH_2PO_4 in 100 mM NaCl and 50 μM EDTA (pH 7.0), and desalted using Sephadex G-25.

Melting Temperature. UV thermal melting profiles were collected as a function of pH with the oligodeoxynucleotides containing either the X^7•C^{18} or the X^7•A^{18} base pair in 100 mM NaCl buffer. The strand concentration was 10 nM. Data were

collected on a Varian Cary 4E spectrometer. The temperature was increased at a rate of 1 °C/min. The temperature and the absorbance at 260 nm were read and stored at 1 min intervals from 10−70 °C.

NMR. NMR experiments were performed at ^{1}H frequencies of 600 and 800 MHz; the data at 800 MHz were collected using a cryogenic probe. Samples were at 1.0 mM strand concentration. Samples for the nonexchangeable protons were dissolved in 10 mM NaH_2PO_4, 100 mM NaCl, and 50 μM Na_2EDTA (pH 7.0) to a volume of 280 μL. They were exchanged with D_2O and suspended in 280 μL of 99.996% D_2O. The pH was adjusted using dilute DCl or NaOD. The temperature was 15 °C. Samples for the observation of exchangeable protons were dissolved in 280 μL of the same buffer containing 9:1 H_2O:D_2O (v/v). The temperature was 5 °C. The ^{1}H chemical shifts were referenced to water. Data were processed using FELIX 2000 (Accelrys Inc., San Diego, CA) on UNIX workstations (Dell Inc., Austin, TX). For all experiments, a relaxation delay of 1.5 s was used. The nuclear Overhauser effect spectroscopy (NOESY) spectra were recorded with 512 real data in the *t*2 dimension and 2048 real data in the *t*1 dimension. For assignment of exchangeable protons, NOESY experiments used the Watergate solvent suppression scheme (*63*). The mixing time was 250 ms. The spectrum was zero-filled during processing to create a matrix of 1024 × 512 real points. For assignment of nonexchangeable protons and the derivation of distance restraints, NOESY experiments used TPPI quadrature detection, and mixing times of 60, 150, 200, and 250 ms were used. The spectra were zero-filled during processing to create a matrix of 1024 × 1024 real points. The double-quantum filtered correlation spectroscopy (DQF-COSY) experiments were performed with TPPI quadrature detection and presaturation of the residual water during the relaxation delay. ^{1}H−^{31}P HMBC spectra (*64, 65*) were obtained at 25 °C. The data matrix was 96 (*t*1) × 1024 (*t*2) complex points. The data were Fourier transformed after zero filling in the *t*1 dimension, resulting in a matrix size of 128 (*D*1) × 512 (*D*2) real points. The ^{31}P chemical shifts were not calibrated.

Restraints. Footprints were drawn around cross-peaks obtained at a mixing time of 250 ms using FELIX2000. Identical footprints were transferred and fit to the corresponding cross-peaks obtained at the other two mixing times. Cross-peak intensities were determined by volume integrations. These were combined as necessary with intensities generated from complete relaxation matrix analysis of a starting structure to generate a hybrid intensity matrix (*66, 67*). MARDIGRAS (*68*−*70*) iteratively refined the hybrid intensity matrix and optimized agreement between calculated and experimental nuclear Overhauser effect (NOE) intensities. The RANDMARDI algorithm carried out 50 iterations for each set of data, randomizing peak volumes within limits specified by the input noise level (*70*). Calculations were initiated using isotropic correlation times of 2, 3, and 4 ns, and with both A form and B form starting structures and the three mixing times, yielding 18 sets of distances. Analysis of these data yielded experimental distance restraints used in subsequent rMD calculations and the corresponding standard deviations for the distance restraints.

Deoxyribose pseudorotational angles (*P*) were estimated by examining the $^3J_{HH}$ of sugar protons (*71*). The $J_{1'-2'}$ and $J_{1'-2''}$ couplings were measured from ECOSY spectra, while the intensities of H2″-H3′ and H3′-H4′ cross-peaks were determined from DQF-COSY spectra. The data were fit to curves relating the coupling constants to the deoxyribose pseudorotation (P), sugar pucker amplitude (ϕ), and the percentage S type conformation. The pseudorotation and amplitude ranges were converted to the five dihedral angles υ_0 to υ_4. Coupling constants measured from ^{1}H−^{31}P HMBC spectra were applied (*72, 73*) to the Karplus relationship (*74*) to determine the backbone dihedral angle ε (C4′-C3′-O3′-P), related to the H3′-C3′-O3′-P angle by a 120° shift. The ζ (C3′-O3′-P-O5′) backbone angles were calculated from the correlation between ε and ζ in B-DNA.

rMD Calculations. The HNE-adducted duplexes, either in A form or B form DNA helical coordinates, were constructed by bonding the stereospecific HNE C1 and C3 to G[7] N1 and G[7] N^2, respectively using Insight II. The partial charges on the HNE atoms were obtained from density function theory (DFT) calculations using a neutral total charge, utilizing B3LYP/6-31G* basis set and the program GAUSSIAN (*75*). To obtain the A form and B form starting structures that were used for subsequent restrained molecular dynamics (rMD) calculations, these A form or B form modified duplexes were energy minimized using 200 iterations with the conjugate gradients algorithm, in the absence of experimental restraints.

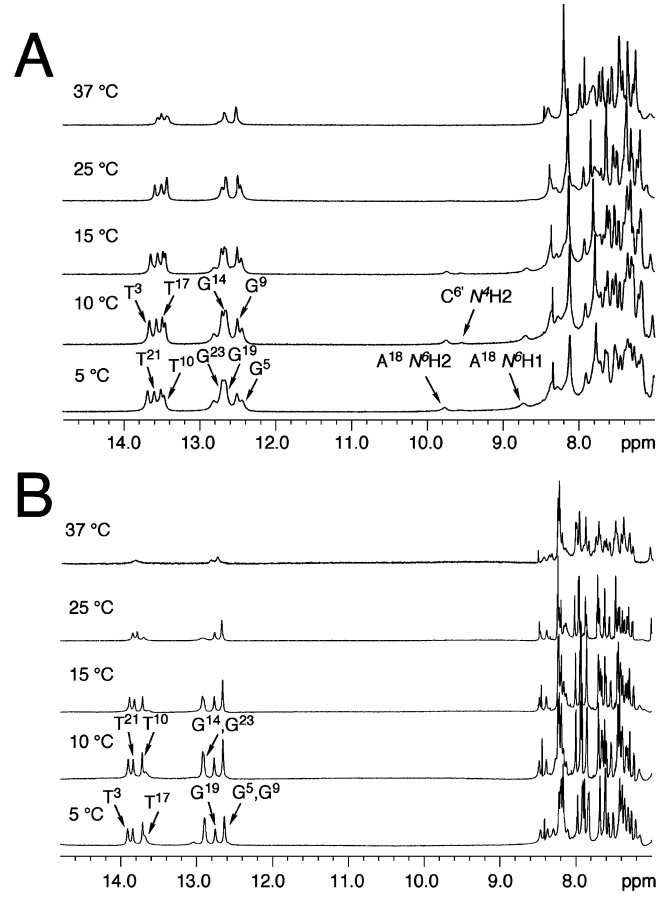

Figure 2. (A) ^{1}H NMR spectra of the mismatched duplex at different temperatures at pH 5.5. Two small resonances at ∼9.8 and 8.8 ppm at low temperature were assigned to the hydrogen-bonded and nonhydrogen-bonded amino protons of the protonated A^{18}. The small peak at ∼9.6 ppm was assigned to the partially protonated C^6 hydrogen-bonded amino proton. (B) ^{1}H NMR of the mismatched duplex at different temperatures at pH 8.9. The broad resonance at ∼13.7 ppm was tentatively assigned to the T^{17} imine proton.

Distance restraints were divided into classes weighted according to the error assessed in their measurements. Class 1, class 2, class 3, class 4, and class 5 were calculated from completely resolved, somewhat overlapped, slightly overlapped, medium overlapped, or heavily overlapped cross-peaks, respectively, which were at least 0.5 ppm from the water resonance or the diagonal line of the spectrum. Class 5 also included all other cross-peaks. NOEs that did not have a distance calculated by MARDIGRAS were estimated by the relative peak intensities. The spectroscopic data indicated that the duplexes conserved Watson−Crick base pairing, so empirical restraints preserving Watson−Crick hydrogen bonding and preventing propeller twisting between base pairs were used (*76*). Empirical backbone and deoxyribose torsion angle restraints derived from B-DNA were used (*77*). The potential energy wells associated with the dihedral angle restraints were ±30°. The force constants of the restraints were scaled from 3.2 to 32 kcal mol^{-1} Å^{-2} during the first 10 ps and were maintained at 32 kcal mol^{-1} Å^{-2} for the remainder of the simulations.

Ten sets of randomly seeded rMD calculations (five from A and five from B type DNA starting structures) were conducted using the program AMBER (version 8.0) (*78*) and the parm99 force field.

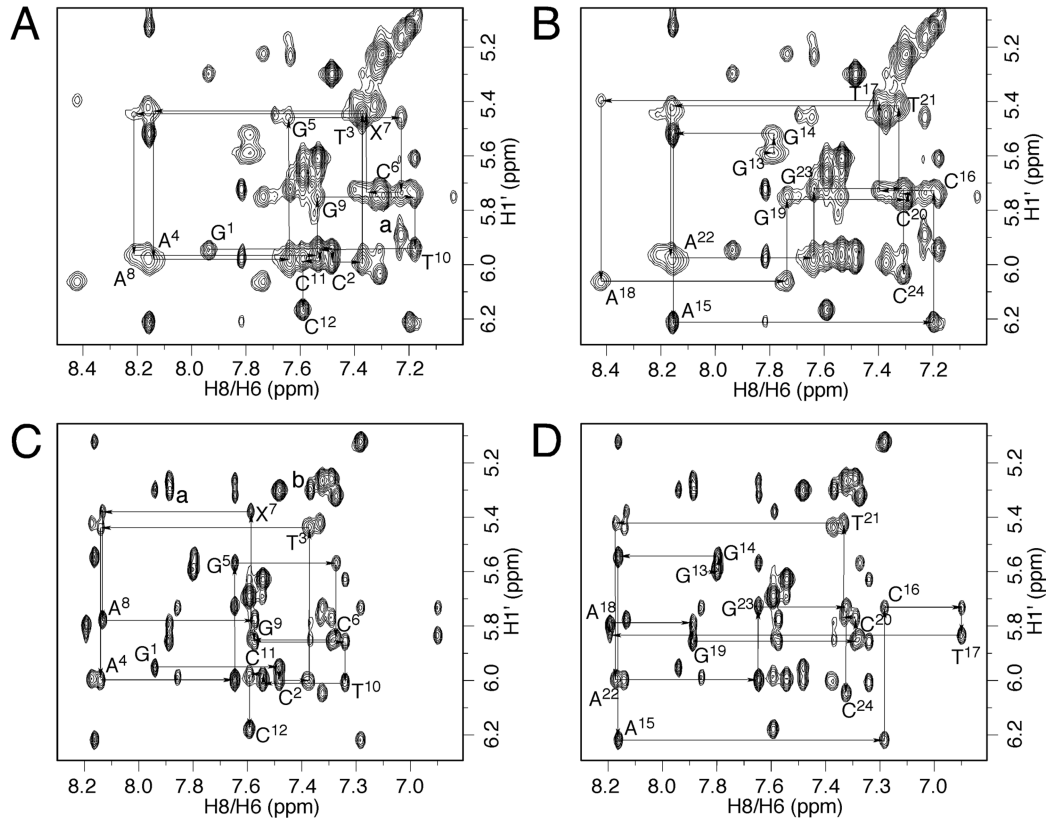

Figure 3. Expansions of NOESY spectra (250 ms) of the mismatched duplex showing the sequential connectivity of the base aromatic protons with sugar H1′ protons. (A) Modified strand at pH 5.5. The strong cross-peak designated as peak "a" was assigned to the C^6 H6→X^7 H8 correlation. (B) Complementary strand at pH 5.5. (C) Modified strand at pH 8.9. Extra cross-peaks designated as peaks "a" and "b" were assigned to the A^8 H2→X^7 H8 and A^{18} H2→X^7 H8 correlations, respectively. (D) Complementary strand at pH 8.9.

The Hawkins, Cramer, Truhlar pairwise generalized Born (GB) model (*79, 80*) was used to simulate implicit waters. The parameters developed by Tsui and Case (*81*) were used. The cutoff radius for nonbonding interactions was 18 Å. The restraint energy function contained terms describing distance and torsion angle restraints, both in the form of square well potentials. Bond lengths involving hydrogens were fixed with the SHAKE algorithm (*82*). A 1000-step energy minimization was performed with an integrator time of 1 fs without experimental restraints, followed by a 100000-iteration simulated annealing protocol with an integrator time step of 1 fs. The system was heated to 600 K in 5000 iterations and kept at 600 K for 5000 iterations, then cooled to 100 K with a time constant of 4.0 ps over 80000 iterations. A final cooling was applied to relax the system to 0 K with a time constant of 1.0 ps over 10000 iterations.

Convergence was assessed for structures having the lowest number of deviations from the experimental distance and dihedral restraints, lowest van der Waals energies, and the lowest overall energies. Finally, the 10 refined structures were energy minimized for 250 iterations without restraints to obtain average structures. The program CORMA (*67*) was utilized to calculate the predicted NOE intensities from the structures refined from rMD calculations. Input volumes (intensities) were normalized from the intensities of protons with fixed intranuclear distances (i.e., cytosine H5−H6 and thymine CH_3−H6 distances). Random noise was added to all intensities to simulate spectral noise. An isotropic correlation time (τ_c) of 3 ns was used. The rotation of thymidine CH_3 groups was modeled using a three-jump site model (*83*). A sixth root residual (R_1^x) factor (*84*) was calculated for each structure. Helicoidal analysis was carried out with the program 3DNA (*85*).

Results

Characterization of the Mismatched Duplex. The 5′-d(GCTAGCXAGTCC)-3′•5′-d(GGACTAGCTAGC)-3′ (X = 1,N^2-HNE-dGuo) oligodeoxynucleotide was characterized by MALDI-TOF mass spectrometry, capillary gel electrophoresis, and C-18 HPLC. It was obtained at >95% purity. However, at pH 7.3, two sets of NMR resonances that exhibited exchange cross-peaks on the NMR time scale were observed. The data suggested that the mismatched duplex adopted two conformations. The COSY spectra exhibited seven cytosine H5→H6 correlations in acidic, neutral, or basic solutions. The COSY spectra at neutral or basic conditions were similar, suggesting that the major conformation in neutral solution was similar to that in basic solution. Furthermore, the C^6 H5→H6 correlation was broad in acidic and neutral solutions whereas it was sharp in basic solution, suggesting in the acidic and neutral solutions that the mismatched duplex underwent a slow conformational exchange involving the adduct region. Shifting the pH to 5.5 or to 8.9 yielded spectra suitable for structural refinement. The resolution of the NMR spectra in acidic solution remained somewhat compromised by resonance broadening, but resonance assignments could be made. The resolutions of NMR spectra obtained in basic solution were outstanding. Hence, subsequent NMR experiments were performed at either acidic or basic pH, in an effort to characterize the two conformational species that were present in equilibrium at neutral pH.

Mismatched X·A Duplex at pH 5.5. Thermal Melting (T_m) Experiments. The T_m of the mismatched duplex at pH 5.5 was 37 °C, lower than that of the corresponding duplex containing X^7•C^{18} base pair, which was 40 °C. ^{1}H NMR spectra of the mismatched duplex at different temperatures in acidic solution are shown in Figure 2A. No imino resonance was assigned to X^7. The imino resonances of the neighboring C^6•G^{19} and A^8•T^{17} base pairs broadened more rapidly than did the imino resonances of the nucleotides located in the middle of the duplex.

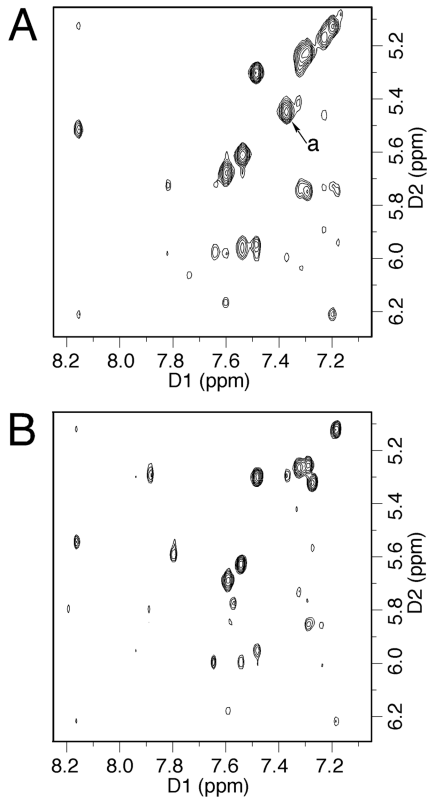

Figure 4. Expansions of NOESY spectra (60 ms) of the mismatched duplex. (A) At pH 5.5, the strong X^7 H2→X^7 H1′ correlation (peak "a") suggested that X^7 adopted the *syn* conformation about the glycosyl bond. (B) The corresponding spectrum at pH 8.9.

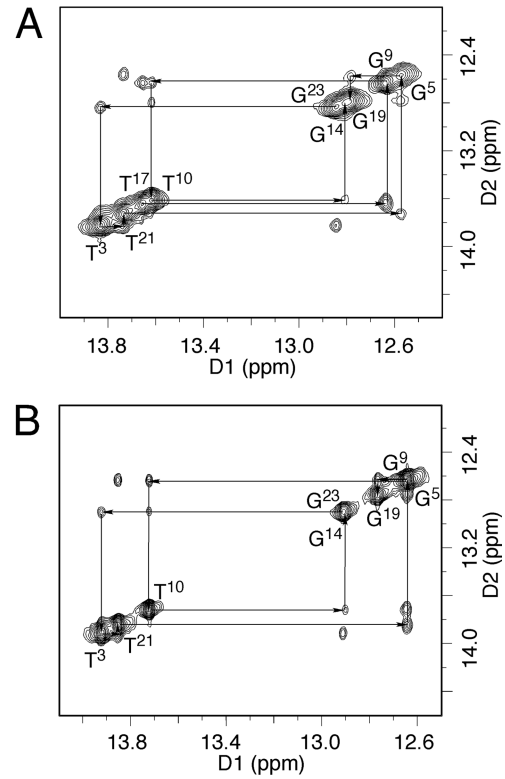

Figure 5. NOE connectivity of the base imino protons. (A) The NOE spectrum at pH 5.5. (B) The NOE spectrum at pH 8.9. No imino resonance was observed for X^7 in either spectrum, indicating that X^7 maintained the 1,N^2-HNE-dGuo structure. The T^{17} imino proton was also missing at pH 8.9.

Nonexchangeable Protons. The sequential NOE assignment of the nonexchangeable protons was accomplished using standard protocols (*86, 87*). The sequential NOEs between the aromatic (note that the X^7 aromatic proton is designated as H2) and the anomeric protons are displayed in Figure 3A,B. Complete sequential NOESY connectivities without an interruption were observed for both modified and complementary strands. Notably, A^{18} H8 was the most downfield among the adenine aromatic protons, and X^7 H2 was the most upfield among the guanine aromatic protons. The A^{18} H8 and A^{18} H2 resonances were observed at 8.42 and 7.03 ppm. These peaks became weaker at pH 7.3 and disappeared at pH 8.9. The T^{17} H6 resonance was observed at 7.37 ppm.

The C^6 H1′→X^7 H2, X^7 H1′→A^8 H8, and T^{17} H1′→A^{18} H8 NOEs were weaker as compared to other internucleotide deoxyribose H1′→purine H8 NOEs. In contrast, the X^7 H2→X^7 H1′ NOE, which overlapped with the T^3 H6→T^3 H1′ NOE, was very strong. The overlapped NOE cross-peak was comparable in intensity to the cytosine H5→H6 correlations in the spectrum with 60 ms mixing time (Figure 4A). The deoxyribose sugar proton resonances were assigned by utilizing a combination of DQF-COSY and NOESY spectra. As compared with the other H2′ protons, X^7 H2′ shifted downfield. The assignments of the nonexchangeable protons are provided in Table S1 in the Supporting Information.

Exchangeable Protons. The base imino protons were assigned based on their sequential connectivities in NOESY spectra (Figure 5A), and these assignments were supported by their NOE cross-peaks to Watson−Crick base-paired amino protons (*88*). Because the X^7 imino resonance was missing, no NOEs arising from the X^7 imino proton were observed. The mismatched duplex exhibited two broad resonances at ∼9.8 and ∼8.8 ppm at low temperatures. They broadened further at higher temperature and disappeared at 25 °C (Figure 2A). These resonances had NOE correlations with T^{17} CH_3, T^{17} N3H, G^{19} N1H, and G^{19} N^2H and were assigned to hydrogen-bonded and nonbonded amino protons of the protonated A^{18}, respectively (*76*). Another weak resonance was observed at ∼9.6 ppm at low temperature (Figure 2A). It was also temperature-dependent and exhibited a weak NOE correlation with the resonance at 8.55 ppm at 5 °C. These two resonances were assigned to the amino protons of the partially protonated C^6 (*89*). The NOE cross-peaks of the imino protons arising from Watson−Crick base pairing for C^2•G^{23}, T^3•A^{22}, A^4•T^{21}, G^5•C^{20}, C^6•G^{19}, A^8•T^{17}, G^9•C^{16}, T^{10}•A^{15}, and C^{11}•G^{14} base pairs were observed.

HNE Protons. X^7 H8 exhibited strong NOE correlations with C^6 H6 (Figure 3A) and C^6 H5 (Figure 6A). Other HNE protons were assigned based on the NOE correlations with 60 ms mixing time (Figure 6A). The resonances of X^7 H7 geminal protons were well-resolved. X^7 $H7^{\alpha}$, which was in the *cis*-configuration with respect to X^7 H8, exhibited a relatively stronger NOE with X^7 H8. X^7 $H7^{\beta}$, which was in the *trans*-configuration with respect to X^7 H8, had a relatively weaker correlation with X^7 H8. X^7 H6 exhibited strong NOEs with the X^7 H7 and X^7 H11 protons. X^7 H11 had strong NOE correlations with X^7 H12 and relatively weaker correlations with X^7 H13. X^7 H16 was the most upfield and exhibited a strong NOE cross-peak with X^7 H15. X^7 H14 was overlapped with X^7 $H7^{\alpha}$. It exhibited strong NOE correlations with X^7 H13 and X^7 H15. These assignments were supported by COSY, DQF-COSY, total correlation spectroscopy (TOCSY), and NOE correlations with nucleotide protons. The chemical shifts of the HNE protons are summarized in Table 1. Notably, the HNE protons exhibited NOE correlations with the C^6 H5 and C^6 H6 protons in the mismatched duplex.

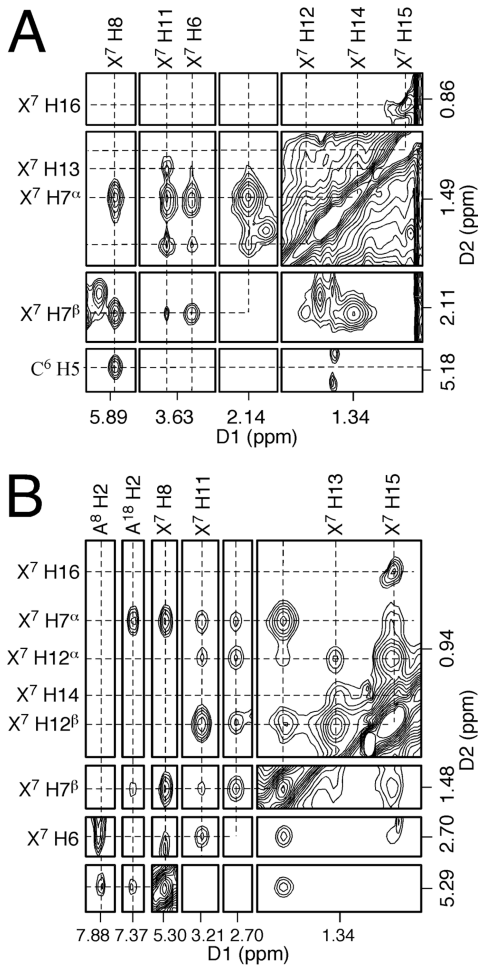

Figure 6. Assignments of HNE protons based on the NOE correlations (60 ms). (A) The NOE spectrum at pH 5.5. (B) The NOE spectrum at pH 8.9.

Table 1. Chemical Shifts of HNE Protons and Related NOEs at pH 5.5 Converted to rMD Distance Restraints

proton	δ (ppm)	NOEs[a]
H6	3.59	C^6 H6 (w), C^6 H3′ (w), X^7 H7$^\alpha$ (s), X^7 H7$^\beta$ (s), X^7 H8 (s), X^7 H12 (m), X^7 H13 (m), X^7 H14 (m), X^7 H15 (m)
H7$^\alpha$	1.49	C^6 H5 (m), C^6 H6 (m), C^6 H1′ (w), C^6 H3′ (w), X^7 H7$^\beta$ (s), X^7 H8 (s), X^7 H11 (m)
H7$^\beta$	2.13	C^6 H5 (m), C^6 H6 (m), C^6 H1′ (w), C^6 H3′ (w), X^7 H8 (s), X^7 H11 (m), X^7 H12 (m), X^7 H13 (w)
H8	5.89	C^6 H5 (s), C^6 H6 (m), C^6 H2′ (m), C^6 H5′ (w), X^7 H11 (m), X^7 H12 (m), X^7 H13 (w), X^7 H15 (w)
H11	3.66	C^6 H6 (w), C^6 H3′ (w), X^7 H12 (m), X^7 H13 (m), X^7 H14 (m), X^7 H15 (m)
H12	1.65	C^6 H6 (w), C^6 H3′ (w), X^7 H13 (s), X^7 H14 (s), X^7 H15 (m)
H13	1.40	C^6 H3′ (w), X^7 H14 (s), X^7 H16 (m)
H14	1.48	C^6 H3′ (m), X^7 H15 (s)
H15	1.33	C^6 H3′ (m), X^7 H16 (s)
H16	0.88	

[a] Letters in brackets indicate peak intensity: s, strong; m, medium; and w, weak.

Deoxyribose and Backbone Angle Conformations. Deoxyribose and backbone angle conformations were determined spectroscopically by DQF-COSY and ^{31}P−H3′ HMBC correlations. Evaluation of the DQF-COSY spectrum revealed that the pseudorotation of the sugar rings of all nucleotides except X^7 and A^{18} was either $C_{1'}$-*exo* or $C_{2'}$-*endo*.

Structural Refinement. A total of 414 distance restraints, including 239 intranucleotide and 175 internucleotide restraints, were calculated from the intensities of NOE cross-peaks by MARDIGRAS. A total of 49 NOEs were assigned to HNE protons (Table 1). In addition, 50 empirical distance restraints defining Watson−Crick base pairing were used; their use was predicated upon inspection of the NMR data, which indicated that Watson−Crick base pairing was intact throughout the duplex except at the X^7•A^{18} base pair. Finally, an additional 180 empirical backbone torsion angle restraints were used; these were based upon inspection of the NMR data, which suggested that the adducted duplex maintained the B type architecture. The A^{18} imino nitrogen N1 was protonated to allow formation of a hydrogen bond with X^7, and empirical distance restraints were used to position the hydrogen bonds of the protonated X^7•A^{18} base pair. Torsion angle restraints were not used at the protonated X^7•A^{18} base pair (Table 2).

Table 2. rMD Restraints and Statistical Analysis of rMD Converged Structures of the Mismatched Duplexes in Acidic and Basic Solutions[a]

solution pH	pH 5.5	pH 8.9
total restraints for rMD calculation	644	671
experimental NOE distance restraints	414	467
intraresidue NOE restraints	239	251
interresidue NOE restraints	175	216
restraints of HNE unit	49	83
empirical base pair restraints	50	44
empirical torsion angle restraints	180	160
backbone torsion angles restraints	90	80
sugar torsion angles restraints	90	80
structure statistics[b]		
NMR R factor (R_1^x) ($\times 10^{-2}$)[c]	7.83	8.77
intraresidue NOEs	7.66	8.08
interresidue NOEs	8.08	9.69
rmsd deviation of refined structures	0.50	0.52

[a] $R_1^x = \sum|(a_0)_i^{1/6} - (a_c)_i^{1/6}|/|(a_0)_i^{1/6}|$, where (a_0) and (a_c) are the intensities of observed (nonzero) and calculated NOE cross-peaks, respectively. [b] HNE unit considered to be a single residue attached to guanine G^7 in the rMD calculation and the statistical analysis. [c] The mixing time used to calculate R_1^x was 250 ms.

The randomly seeded rMD calculations were performed starting with initial structures, which were created either with A or B form geometries. Pairwise rmsd analysis of emergent structures indicated that the calculations converged, irrespective of starting structure (Table 2). The accuracies of the emergent structures were evaluated by comparison of theoretical NOE intensities calculated by complete relaxation analysis for the refined structure, to the experimental NOE intensities, to yield sixth root residuals (R_1^x). This residual was less 0.1 for the modified duplex (Table 2), indicating that the refined structures provided an accurate depiction of the data.

Analysis of rMD Structures. The backbone torsion angles of the refined structures showed the oligodeoxynucleotide remained in the B type geometry except for the adducted region. Expanded views of the average structure around the adducted region are shown in Figure 7A,B, and the base stacking at the modified region is demonstrated in Figure 8A,B. All nucleosides except X^7 maintained the *anti* conformation about the glycosyl bond. The neighboring C^6•G^{19} and A^8•T^{17} base pairs were distorted, but Watson−Crick hydrogen bonding was conserved. X^7 adopted the *syn* conformation about the glycosyl bond, and the χ torsion angle (O4′−C1′−N3−C2) was 106°. The protonated A^{18} adopted the *anti* conformation about the glycosyl bond and formed hydrogen bonds with X^7. The HNE was located in the major groove and exposed to the solvent.

Mismatched Duplex at pH 8.9. Thermal Melting Experiments. The T_m of the mismatched duplex at pH 8.9 was 32 °C, lower than that of the correctly paired duplex containing the X^7•C^{18} base pair, which was 37 °C. Figure 2B shows the

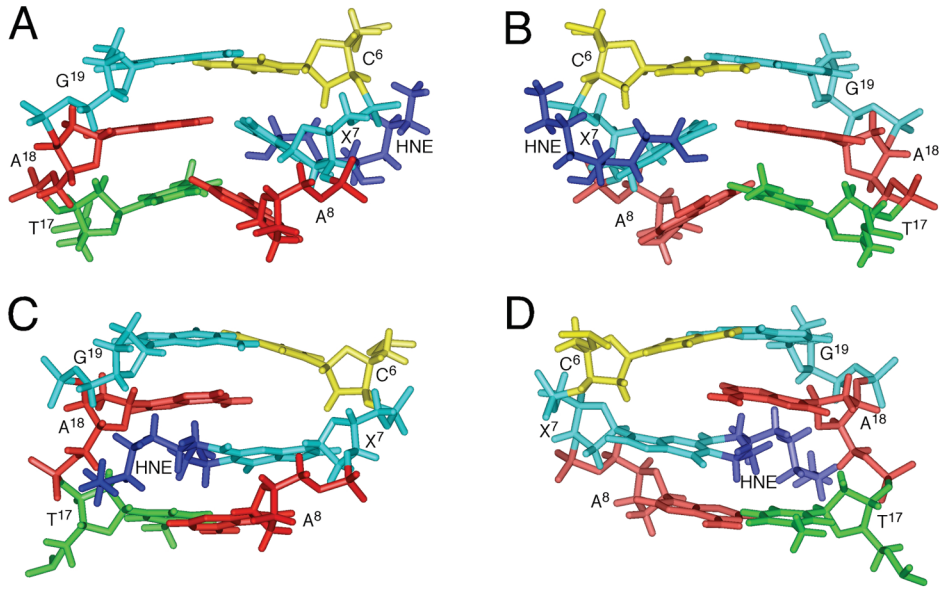

Figure 7. Expanded views of average structures of the mismatched duplex. (A) View from the minor groove at pH 5.5. (B) View from the major groove at pH 5.5. X^7 adopts the *syn* conformation about the glycosyl bond allowing formation of hydrogen bonds with protonated A^{18}. (C) View from the minor groove at pH 8.9. (D) View from the major groove at pH 8.9. X^7 is intercalated and displaces A^{18} in the 5′-direction.

temperature dependence of ^{1}H NMR of the mismatched duplex. No imino resonance was assigned to X^7. The G^{19} imino resonance from the 5′-neighbor C^6•G^{19} base pair broadened more rapidly than the imino resonances of the nucleotides located in the middle of the sequence. A resonance tentatively assigned as the T^{17} imino resonance from the 3′-neighbor A^8•T^{17} base pair was broad even at 5 °C.

Nonexchangeable Protons. The sequential NOE assignment of the nonexchangeable protons was also accomplished using standard protocols (*86, 87*). The sequential NOEs between the aromatic and the anomeric protons are displayed in Figure 3C,D. Complete sequential NOESY connectivities without interruption or peak intensity differences were observed for both the modified and the complementary strands. The deoxyribose sugar proton resonances were assigned by utilizing a combination of DQF-COSY and NOESY spectra. The resonances of A^{18} H8 and A^8 H2 were found at 8.20 and 7.89 ppm, respectively. In addition, a singlet at 6.91 ppm was assigned to T^{17} H6. It became smaller at pH 7.3 and almost disappeared at pH 5.5. The assignments of the nonexchangeable protons are provided in Table S2 in the Supporting Information.

The chemical shifts of the mismatched duplex in basic solution were compared with the corresponding unmodified G^7•A^{18} mismatched duplex. Large chemical shift perturbations were located at the adducted X^7•A^{18} base pair and the neighboring C^6•G^{19} and A^8•T^{17} base pairs, indicating some perturbation at the adduct region. The chemical shifts were also compared with those in acidic solution. Large differences were also observed at the modified X^7•A^{18} base pair and the neighboring C^6•G^{19} and A^8•T^{17} base pairs, suggesting large conformational differences between acidic and basic solutions were located at the adduct region.

Exchangeable Protons. The resonances of the base imino protons were assigned based on their sequential connectivty in NOESY spectra (Figure 5B) and were supported by their NOE cross-peaks to Watson−Crick hydrogen-bonded amino protons (*88*). X^7 was not assigned an imino resonance. The T^{17} N3H resonance could not be assigned, although a broad resonance at ∼13.7 ppm was observed (Figure 2B) and located in the thymine imino region of the spectrum. The NOE cross-peaks of the imino protons arising from Watson−Crick base pairing for C^2•G^{23}, T^3•A^{22}, A^4•T^{21}, G^5•C^{20}, C^6•G^{19}, G^9•C^{16}, T^{10}•A^{15}, and C^{11}•G^{14} base pairs were observed.

HNE Protons. X^7 H8 exhibited strong NOEs with A^8 H2 and A^{18} H2 (Figure 3C). Other HNE protons were also assigned based on the NOE correlations and the peak intensities at 60 ms mixing time (Figure 6B). In addition to the resonances of the geminal X^7 H7 protons, the X^7 H12 geminal protons were also resolved. The assignments were supported by COSY, DQF-COSY, TOCSY, and NOE correlations with nucleotide protons. The chemical shifts of the HNE protons are summarized in Table 3. As compared with those at pH 5.5, the resonances of the HNE protons were shifted upfield. NOE cross-peaks were assigned to HNE protons (Table 3). HNE protons were found to exhibit NOE interactions with minor groove protons, including A^8 H2, A^{18} H2, and A^{18} H1′.

Deoxyribose and Backbone Angle Conformations. Deoxyribose and backbone angle conformations were determined spectroscopically from DQF-COSY and ^{31}P−H3′ HMBC correlations. Evaluation of the DQF-COSY spectrum revealed that the pseudorotation of the sugar rings of all nucleotides except X^7 and A^{18} was either C_1′-*exo* or C_2′-*endo*. The T^{17} phosphate resonance shifted downfield.

Structural Refinement. A total of 467 distance restraints, including 251 intraresidue and 216 interresidue restraints, were calculated from the intensities of NOE cross-peaks by MARDIGRAS. In addition, 44 empirical distance restraints defining Watson−Crick base pairing were used to refine the structure of the duplex; their use was predicated upon inspection of the NMR data, which indicated that Watson−Crick base pairing was intact throughout the duplex except for the X^7•A^{18} and A^8•T^{17} base pairs. Finally, an additional 160 empirical backbone torsion angle restraints were also used for structure refinement; these were based upon inspection of the NMR data, which suggested that the adducted duplex maintained the B type architecture. Hydrogen bonding and torsion angle restraints were not used for the X^7•A^{18} and A^8•T^{17} base pairs (Table 2). The randomly seeded rMD calculations were performed starting with initial structures, which were created either with A or B form geometries. Pairwise rmsd analysis of emergent structures indicated that the calculations converged, irrespective of starting structure (Table 2). The accuracies of the emergent structures

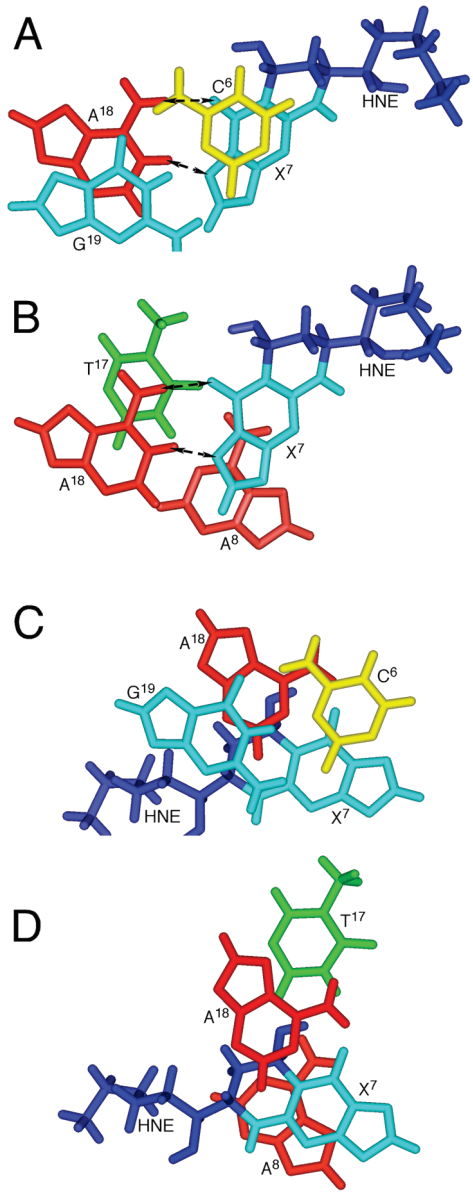

Figure 8. (A, B) Base stacking of the mismatched duplex at pH 5.5. The dashed arrows indicate the potential hydrogen bonds of the X^7•A^{18} mismatched base pair. (C, D) Base stacking of the mismatched duplex at pH 8.9. No hydrogen bond is formed for the mismatched X^7•A^{18} or A^8•T^{17} base pairs.

were evaluated by comparison of theoretical NOE intensities calculated by complete relaxation analysis for the refined structure, to the experimental NOE intensities, to yield sixth root residuals (R_1^x). This residual was less than 0.1 for the modified duplex (Table 2), indicating that the refined structures provided an accurate depiction of the data.

Analysis of the rMD Structure. The backbone torsion angles of the refined structures showed that the oligodeoxynucleotide remained in the B type geometry except at the adduct region. Expanded views of the average structure around the adduct region are shown in Figure 7C,D, and the base stacking around the modified region is shown in Figure 8C,D. All nucleosides including X^7 maintained the *anti* conformation about the glycosyl bond. However, the duplex was highly perturbed. X^7 was intercalated into the duplex, and the complementary A^{18} was displaced in the 5′-direction. No hydrogen bond was observed between them. The neighboring C^6•G^{19} base pair maintained Watson−Crick hydrogen bonding with minimal distortion. The A^8•T^{17} base pair was also highly perturbed, and

Table 3. Chemical Shifts of HNE Protons and Related NOEs at pH 8.9 Converted to rMD Distance Restraints

proton	δ (ppm)	NOEs[a]
H6	2.70	X^7 H7$^\alpha$ (m), X7 H7$^\beta$ (s), X^7 H8 (m), X^7 H11 (s), X^7 H12$^\alpha$ (m), X^7 H12$^\beta$ (s), X^7 H13 (w), X^7 H14 (w), A^{18} H2 (m)
H7$^\alpha$	0.95	X^7 H7$^\beta$ (s), X^7 H8 (s), X^7 H11 (m), X^7 H12$^\beta$ (m), X^7 H13 (m), A^8 H2 (w), T^{17} H1′ (w), A^{18} H2 (m), A^{18} H1′ (w), A^{18} H4′ (w)
H7$^\beta$	1.48	X^7 H8 (s), X^7 H11 (m), X^7 H12$^\alpha$ (s), X^7 H12$^\beta$ (s), X^7 H13 (m), X^7 H14 (w), A^8 H2 (w), A^{18} H2 (m), A^{18} H1′ (w), A^{18} H4′ (w)
H8	5.30	X^7 H11 (m), X^7 H12$^\alpha$ (m), X^7 H12$^\beta$ (m), X^7 H13 (w), A^8 H2 (m), T^{17} H1′ (w), A^{18} H2 (m), A^{18} H1′ (w)
H11	3.21	X^7 H12$^\alpha$ (m), X^7 H12$^\beta$ (s), X^7 H13 (m), X^7 H14 (m), A^{18} H2 (m), A^{18} H4′ (w)
H12$^\alpha$	1.04	X^7 H12$^\beta$ (s), X^7 H13 (s), A^{18} H2 (w), A^{18} H1′ (w), A^{18} H4′ (m), A^{18} H5′ (w), G^{19} H4′ (w), G^{19} H5′ (w)
H12$^\beta$	1.21	X^7 H13 (s), A^8 H2 (w), A^{18} H2 (m), A^{18} H8 (w), A^{18} H1′ (w), A^{18} H4′ (m), A^{18} H5′ (w), G^{19} H4′ (w), G^{19} H5′ (w)
H13	1.36	X^7 H14 (s), X^7 H15 (m), X^7 H16 (w), A^{18} H2 (w), A^{18} H4′ (m), A^{18} H5′ (w), G^{19} H4′ (m)
H14	1.14	X^7 H16 (m), A^{18} H2 (w), A^{18} H4′ (m), A^{18} H5′ (w), A^{18} H5″ (w), G^{19} H4′ (w), G^{19} H5′ (w)
H15	1.21	X^7 H16 (s), A^{18} H4′ (m), A^{18} H5′ (m), A^{18} H5″ (m), G^{19} H4′ (m), G^{19} H5′ (m)
H16	0.82	G^9 H5′ (w), A^{18} H4′ (w), G^{19} H1′ (w), G^{19} H4′ (w), G^{19} H5′ (w)

[a] Letters in brackets indicate peak intensity: s, strong; m, medium; and w, weak.

no hydrogen bond was formed between these nucleotides. The aliphatic HNE chain was oriented toward the minor groove.

Discussion

(6*S*,8*R*,11*S*) 1,N^2-HNE-dGuo Adduct Does Not Undergo Ring Opening When Placed Opposite dAdo in Duplex DNA. The ring-closed (6*S*,8*R*,11*S*) 1,N^2-HNE-dG adduct in duplex DNA opposite a mismatched dA contrasts with the situation when the same adduct is placed opposite the correct complementary nucleotide dCyd in this sequence. In the latter instance, the exocyclic ring of the (6*S*,8*R*,11*S*) 1,N^2-HNE-dG adduct undergoes ring opening and exists primarily as a diastereomeric set of minor groove cyclic hemiacetals (*36*). The conclusion that the (6*S*,8*R*,11*S*) exocyclic 1,N^2-dGuo adduct does not undergo ring opening when placed opposite dA derives, in part, from the failure to observe the X^7 N9H imino resonance in acidic, neutral, or basic solutions (Figure 5). The alternative possibility that ring opening had occurred but that the resulting X^7 N9H imino resonance was in rapid exchange with solvent, and hence was not observed, was considered. However, no spectroscopic evidence for a ring-opened aldehydic proton is observed, under acidic, neutral, or basic solution conditions. An aldehydic ^{1}H resonance was observed when this adduct was placed opposite the correct complementary nucleotide dCyd nucleotide in this sequence, even though it existed primarily as a diastereomeric set of minor groove cyclic hemiacetals (*36*). Moreover, the data of the present case suggest that the bulky ring-closed (6*S*,8*R*,11*S*) 1,N^2-HNE-dGuo adduct rotates about the glycosyl bond, into the *syn* conformation under acidic conditions; this is supported by the observation of NOEs with major groove protons, which would not be anticipated if ring opening of the bulky lesion to the corresponding minor groove cyclic hemiacetal forms were present (*36*). Additionally, the chemical shifts of X^7 H6−H8 and H11 are similar to those observed for the exocyclic 1,N^2-dGuo nucleotide (*35*) (Table

Table 4. Comparison of the Chemical Shifts of the HNE Protons

sequence	X^{7a}	X^7•C^{18b}	X^7•A^{18}	
solution	methanol	pH 7.0	pH 5.5	pH 8.9
H6	3.61	4.55	3.59	2.70
H7$^{\alpha}$	1.60	2.17	1.49	0.95
H7$^{\beta}$	2.19	2.17	2.13	1.48
H8	6.40	5.43	5.89	5.30
H11	3.47	4.23	3.66	3.21

[a] Cited from ref *35*. [b] cited from ref *36*.

4) but differ from the chemical shifts of X^7 H6−H8 and H11 when the adduct exists as diastereomeric N^2-dGuo cyclic hemiacetals when placed complementary to dCyd in duplex DNA (*36*).

The observation that the (6*S*,8*R*,11*S*) 1,N^2-HNE-dGuo adduct maintains the ring-closed structure in DNA when mismatched with dAdo is also consistent with the notion that placement of enal-derived 1,N^2-hydroxypropano-dGuo adducts opposite dCyd in duplex DNA facilitates the ring-opening reaction to aldehydic products. Riggins et al. (*37, 38*) reported mechanistic studies of the ring opening and closing of the related malondialdehyde-derived adduct 3-(2′-deoxy-β-D-erythro-pentofuranosyl)pyrimido-[1,2-α]purin-10(3*H*)-one (M_1dG). They concluded that ring opening of M_1dG as a nucleoside or in oligodeoxynucleotides occurs via a reversible second-order reaction with hydroxide and is catalyzed by the complementary dCyd in duplex DNA. The closure of the resulting N^2-(3-oxo-1-propenyl)-dGuo anion is pH-dependent, and under neutral and acidic conditions, ring closure is biphasic, leading to the rapid formation of intermediates that slowly convert to M_1dG in a general acid-catalyzed reaction, in the presence of dCyd in the complementary strand. It should be noted that the ring-opened N^2-(3-oxo-1-propenyl)-dGuo adduct has a perturbed pK_a (∼6.9) relative to the extended conjugation offered by the N^2-(3-oxo-1-propenyl) group, which is likely to play a significant role in the mechanism of ring opening and closing (*90*). The enal-dGuo adducts are saturated and more likely to have a pK_a similar to dGuo.

Structure of the (6*S*,8*R*,11*S*) 1,N^2-HNE-dGuo Adduct Mismatched with dAdo. Acidic Solution. The (6*S*,8*R*,11*S*) 1,N^2-HNE-dGuo adduct maintains a ring-closed form and rotates about the glycosyl bond into the *syn* conformation with a predicted χ torsion angle at X^7 of 106° when mismatched with dAdo at low pH. The strong X^7 H2→X^7 H1′ NOE correlation, the downfield chemical shift of the X^7 H2′ resonance (*91*−*94*), the upfield chemical shift of X^7 H2 as compared to other guanine H8 resonances, and the observation of X^7 H2→A^8 H2 and X^7 H2→A^{18} H2 NOEs are each consistent with this conclusion. The downfield chemical shifts of A^{18} N^2H, and A^{18} H8 as compared with the other adenines are consistent with the conclusion that A^{18} is protonated (*76, 89, 95, 96*). Similar to the 1,N^2-propano-2′-deoxyguanosine (PdG)•dAdo base pair (*76*), the anticipated far downfield resonance of the protonated A^{18} N1H is not observed, suggesting that A^{18} N1H undergoes rapid exchange with solvent and is probably only weakly hydrogen bonded (Figure 8A,B). The presence of the X^7 *syn* conformation and A^{18} protonation facilitates base pairing through X^7 O^{10}→A^{18} N^6H and X^7 N1→A^{18} N1H hydrogen bonds (note that X^7 N1 corresponds to N7 of unmodified Gua and X^7 O^{10} corresponds to O^6 of unmodified Gua) (Chart 1). The *syn* conformation of the glycosyl torsion angle places the HNE moiety in the major groove (Figure 7A,B), consistent with the NOE correlations with major groove protons, notably C^6 H5 and C^6 H6 (Table 1). The 5′-neighbor C^6•G^{19} and 3′-neighbor A^8•T^{17} base pairs maintain Watson−Crick base pairing but are distorted (Figure 7A,B). This

Chart 1. Hydrogen Bonding of X^7•A^{18} Base Pair in Acidic Solution

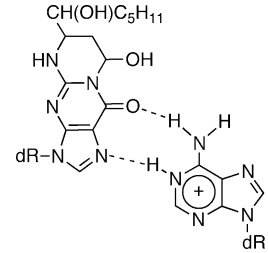

X^7 (*syn*) A^{18} (*anti*)

conclusion is supported by the observation that the T^{17} and G^{19} imino resonances broaden more rapidly as compared to the other imino resonances (Figure 2A).

Basic Solution. In basic solution, all nucleotides including X^7 adopt the *anti* conformation about the glycosyl bond. Thus, the HNE moiety is oriented toward the minor groove (Figure 7C,D). The presence of the *anti* conformation about the glycosyl bond at X^7 disrupts Watson–Crick hydrogen bonding at the adducted base pair (Figure 8C,D) and greatly perturbs the DNA duplex at the lesion site. The rMD calculations predict that the complementary A^{18} is displaced in the 5′-direction, resulting in a bulge at the X^7•A^{18} base pair. The presence of Watson−Crick hydrogen bonding at the 5′-neighboring C^6•G^{19} base pair is supported by the observation of the G^{19} imino resonance and NOEs between the G^{19} imino proton and the exocyclic amino protons of C^6 (Figure 5B). However, these disappear at lower temperatures as compared to other imino resonances (Figure 2B) consistent with the prediction from the rMD calculations that base pair C^6•G^{19} is distorted (Figure 8C). In the 3′-direction, the broad T^{17} imino resonance (Figure 2B) and lack of NOEs to the A^8 N^6H and A^8 H2 resonances lead to the conclusion that base pair A^8•T^{17} is also significantly disrupted (Figure 8D). The downfield shift of the associated ^{31}P resonance suggests that that the phosphodiester backbone is distorted at the lesion site.

Conformational Equilibrium of the Mismatched Duplex in Neutral Solution. At pH 7.3, both the *syn* and the *anti* conformations of X^7 about the glycosyl bond are populated. This conclusion is supported by the observation that two sets of ^{1}H NMR resonances, matching those in acidic and basic solutions, respectively, are obtained at pH 7.3. Exchange NOE cross-peaks are observed for X^7 H2, A^8 H2, T^{17} H6, A^{18} H2, A^{18} H8, and G^{19} H8, indicating a slow exchange between the acidic and the basic conformations of the HNE adduct, on the NMR time scale (Chart 2) (Figure S3 in the Supporting Information). The steric bulk of the HNE aliphatic chain presumably slows the conformational exchange rate. At pH 7.3, the set of resonances corresponding to those observed in basic solution is stronger than are those observed in acidic solution, suggesting the major conformer, which constitutes 60−70% of the overall conformations based on the integration of the ^{1}H resonances, is that in which X^7 adopts the *anti* conformation about the glycosyl bond. This is also supported by the similarity of COSY spectra at pH 7.3 and pH 8.9. The pK_a of adenosine is ∼7.6 (*97*); therefore, A^{18} is largely protonated at pH 5.5, X^7 adopts the *syn* conformation about the glycosyl bond to form hydrogen bonds with A^{18}; A^{18} is weakly protonated at pH 7.3, and the *anti* conformation of the glycosyl bond is the major species present; A^{18} is not protonated at pH 8.9, and the *anti* conformation of the glycosyl bond predominates.

Structure−Activity Relationships. The inability of the (6*S*,8*R*,11*S*) 1,N^2-HNE-dGuo adduct to undergo ring opening

Chart 2. pH-Dependent *syn/anti* Conformational Equilibrium of the Ring-Closed 1,N^2-HNE-dGuo Adduct When Mismatched with dAdo in Duplex DNA

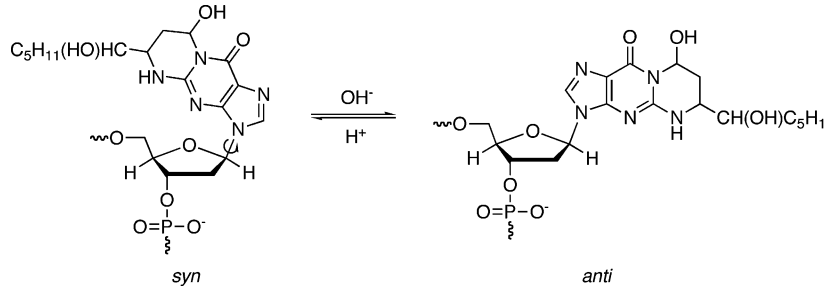

when placed opposite dAdo in duplex DNA suggests that it does not undergo further chemistry. In contrast, when placed complementary to dCyd in this 5′-CpG-3′ sequence, the (6*S*,8*R*,11*S*) adduct slowly forms an interstrand cross-link (*35*). The slow rate of interstrand cross-link formation is attributed to the fact that the (6*S*,8*R*,11*S*) 1,N^2-HNE-dGuo adduct exists primarily as a set of diastereomeric cyclic hemiacetals when placed into this duplex (*36*); these cyclic hemiacetals mask the aldehyde necessary for cross-link formation. In contrast, the corresponding 1,N^2-dGuo adducts of acrolein (*98, 99*) and crotonaldehyde (*99, 100*), which exist predominantly as aldehydes and do not rearrange to cyclic hemiacetals, form interchain cross-links more rapidly when paired opposite dCyd in this sequence context (*99, 101, 102*). In the case of the crotonaldehyde adduct, the 6*R* stereoisomer forms cross-links more efficiently than does the 6*S* stereoisomer (*102, 103*). This is attributed to the relative orientations of the reactive aldehyde species within the minor groove for the two diasteromeric adducts, such that interstrand cross-linking is favored for the 6*R* stereoisomer (*100*). Significantly, the (6*S*,8*R*,11*S*) diastereomeric adduct derived from HNE possesses the same relative stereochemistry as does the 6*R* crotonaldehyde adduct and, likewise, favorably orients the reactive aldehyde species to facilitate interstrand cross-link formation (*104*).

Biological Implications. The low levels of mutations induced by the (6*S*,8*R*,11*S*) 1,N^2-HNE-dGuo adduct when present in duplex DNA opposite cytosine are likely related to the observation that it undergoes ring opening to expose the Watson−Crick hydrogen-bonding face of the adducted dGuo (*58*), which facilitates the correct incorporation of dCTP opposite the lesion during lesion bypass. A similar explanation has been advanced to explain the low levels of mutations induced by the acrolein (*105, 106*) and crotonaldehyde-derived exocyclic 1,N^2-dGuo adducts (*107*). Wolfle et al. (*61*) reported that the sequential activity of pols ι and κ bypassed the (6*S*,8*R*,11*S*) and (6*R*,8*S*,11*R*) 1,N^2-HNE-dG adducts. Significantly, pol ι correctly inserted dCTP and to a lesser extent dTTP opposite the HNE adduct. Further extension was achieved in the presence of pol κ, which elongated from a Cyt opposite the HNE adducts much more efficiently than when Thy was opposite the adducts (*61*).

The source of the G→T transversions induced by the (6*S*,8*R*,11*S*) 1,N^2-HNE-dG adduct in this sequence remains obscure. Xing et al. (*26*) attributed the low levels of G→T transversions to the reorientation of the adduct into the *syn* conformation about the glycosyl bond, thus allowing misincorporation of dATP opposite the lesion. This might allow for subsequent extension from the mismatched template primer, for example, by polymerase ζ, which efficiently extends from primer-terminal base pairs containing mismatches or lesions (*108*). The present structural data confirm that such a reorientation about the glycosyl bond does occur when the (6*S*,8*R*,11*S*) 1,N^2-HNE-dG adduct is mismatched with dAdo in duplex DNA and that the *syn* conformation of the adduct is present in equilibrium with the *anti* conformation at physiological pH values. Xing et al. (*26*) subsequently invoked the transient presence of the rare imine tautomer of dATP during trans-lesion bypass as a potential source of the G→T transversions. In contrast, the present results suggest that a pH-mediated transient protonation of the N1 imine of dAdo occurs in duplex DNA. The (6*S*,8*R*,11*S*) 1,N^2-HNE-dGuo adduct also induces G→A transitions in the human *p53* gene (*55, 57*) and in the sequence used in the present study (*58*). Thus, the extent to which the 1,N^2-HNE-dGuo•Thy mismatched sequence perturbs the DNA duplex will also be of interest. The (6*S*,8*R*,11*S*) HNE-induced adduct is anticipated to also maintain the exocyclic 1,N^2-dGuo structure when mismatched with Thy in the complementary strand.

The saturated PdG adduct, which is stable in the exocyclic 1,N^2-dGuo configuration, provides a surrogate for the chemically unstable enal-derived exocyclic 1,N^2-dGuo adducts (*76, 89, 95, 109*−*115*). The conformation of PdG in either PdG•dCyd (*89, 95*) or PdG•dAdo (*76, 109, 111, 112*) base pairs is also pH-dependent. PdG adopts the *syn* conformation about the glycosyl bond with complementary dCyd or dAdo in acidic solution, whereas it adopts the *anti* conformation without hydrogen bonds with the opposite base in basic solution. At neutral pH or a pK_a value of 7.6, the two conformations exist in equilibrium. Plum et al. (*116*) showed that the PdG lesion alters the differential thermal stability (ΔT_m) but not the differential thermodynamic stability ($\Delta\Delta G$) of duplexes with correctly paired dCyd or mismatched dAdo cross-strand partners. This has led to the suggestion that the observed preference for insertion of dATP over dCTP across from the PdG lesion should not be rationalized in terms of thermodynamic differences between the final duplex states and probably instead reflects properties of the DNA polymerase and the replication fork. Likewise, the present data indicate that the T_m for the X^7•A^{18} base pair in either basic or acidic solution is lower than is the T_m for the X^7•C^{18} base pair. In light of these findings, the structure of the (6*S*,8*R*,11*S*) 1,N^2-HNE-dGuo adduct, particularly in complexes with the bypass polymerases ι and κ (*61*), will be of interest.

A similar pH-dependent *syn/anti* conformational exchange has also been observed for the 1,N^2-ethenodGuo (1,N^2-ϵdG)•dCyd (*117*−*119*) base pair. Similar to the PdG adduct, and differing from the (6*S*,8*R*,11*S*) 1,N^2-HNE-dGuo adduct, 1,N^2-ϵdGuo is stable in the exocyclic ring-closed configuration. Under basic conditions, both 1,N^2-ϵdGuo and the complementary dCyd adopted the *anti* conformation about the glycosyl bonds (*117, 118*). In contrast, under acidic conditions, the 1,N^2-ϵdGuo adduct formed a Hoogsteen pair with the complementary cytosine, characterized by downfield shifts of the amino protons of the cytosine complementary to the exocyclic adduct (*119*).

Summary

The 1,N^2-HNE-dGuo adduct with the (6*S*,8*R*,11*S*) configuration maintains the exocyclic 1,N^2-dGuo structure when mismatched with dAdo in this duplex. It undergoes syn/anti conformational equilibrium with the *anti* conformation being the major species in neutral solution. The *syn* conformation favors base pairing with the complementary protonated A^{18} in acidic solution. In basic solution, X^7 adopts the *anti* conformation about the glycosyl bond without hydrogen bonding with A^{18}. The X^7•A^{18} mismatch greatly perturbs the neighboring C^6•G^{19} and A^8•T^{17} base pairs in both acidic and basic solutions.

Deposition of Structural Data. The PDB files for the mismatched oligodeoxynucleotide duplex structure at pH 5.5 and pH 8.9 are ZKAR and ZKAS, respectively.

Acknowledgment. Dr. Markus Voehler assisted with NMR experiments, and Albena Kozekova assisted with the synthesis of the (6*S*,8*R*,11*S*) HNE-modified oligodeoxynucleotide. This work was supported by NIH Grant PO1 ES-05355 (R.S.L, C.J.R., and M.P.S.). Funding for the NMR spectrometers was supplied by Vanderbilt University, by NIH Grant RR-05805, and the Vanderbilt Center in Molecular Toxicology, ES-00267. The Vanderbilt-Ingram Cancer Center is supported by NIH Grant CA-68485.

Supporting Information Available: Chemical shifts of the mismatched duplex at pH 5.5 (Table S1); chemical shifts of the mismatched duplex at pH 8.9 (Table S2); NOE restraints utilized in the rMD calculation at pH 5.5 (Table S3); NOE restraints utilized in the rMD calculation at pH 8.9 (Table S4); torsion angles of the rMD structure at pH 5.5 (Table S5); torsion angles of the rMD structure at pH 8.9 (Table S6); force field parameters for the 1,N^2-HNE-dGuo adduct (Figure S1); ^{1}H NMRs of the mismatched duplex at pH 5.5, 7.3, and 8.9 (Figure S2); exchange NOE correlations of the two sets of resonances at pH 7.3 (Figure S3); NOE cross-peaks of the imino protons at pH 5.5 and 8.9 (Figure S4); NOE cross-peaks of the protonated A^{18} and C^6 amino protons at pH 5.5 (Figure S5); NOE cross-peaks associated with HNE protons at pH 5.5 and 8.9 (Figure S6); chemical shift perturbations of the mismatched duplex at pH 8.9 (Figure S7); chemical shift comparisons of the mismatched duplex at pH 5.5 and 8.9 (Figure S8); residue-by-residue sixth root residuals (R_1^x) at pH 5.5 and 8.9 (Figure S9); and CPK models of average structures of the mismatched duplex at pH 5.5 and 8.9 (Figure S10). This material is available free of charge via the Internet at http://pubs.acs.org.

References

(1) Benedetti, A., Comporti, M., and Esterbauer, H. (1980) Identification of 4-hydroxynonenal as a cytotoxic product originating from the peroxidation of liver microsomal lipids. *Biochim. Biophys. Acta 620*, 281–296.

(2) Esterbauer, H., Schaur, R. J., and Zollner, H. (1991) Chemistry and biochemistry of 4-hydroxynonenal, malonaldehyde and related aldehydes. *Free Radical Biol. Med. 11*, 81–128.

(3) Burcham, P. C. (1998) Genotoxic lipid peroxidation products: Their DNA damaging properties and role in formation of endogenous DNA adducts. *Mutagenesis 13*, 287–305.

(4) Lee, S. H., and Blair, I. A. (2000) Characterization of 4-oxo-2-nonenal as a novel product of lipid peroxidation. *Chem. Res. Toxicol. 13*, 698–702.

(5) Schneider, C., Tallman, K. A., Porter, N. A., and Brash, A. R. (2001) Two distinct pathways of formation of 4-hydroxynonenal. Mechanisms of nonenzymatic transformation of the 9- and 13-hydroperoxides of linoleic acid to 4-hydroxyalkenals. *J. Biol. Chem. 276*, 20831–20838.

(6) Schneider, C., Porter, N. A., and Brash, A. R. (2008) Routes to 4-hydroxynonenal: Fundamental issues in the mechanisms of lipid peroxidation. *J. Biol. Chem. 283*, 15539–15543.

(7) Nadkarni, D. V., and Sayre, L. M. (1995) Structural definition of early lysine and histidine adduction chemistry of 4-hydroxynonenal. *Chem. Res. Toxicol. 8*, 284–291.

(8) Amarnath, V., Valentine, W. M., Montine, T. J., Patterson, W. H., Amarnath, K., Bassett, C. N., and Graham, D. G. (1998) Reactions of 4-hydroxy-2(*E*)-nonenal and related aldehydes with proteins studied by carbon-13 nuclear magnetic resonance spectroscopy. *Chem. Res. Toxicol. 11*, 317–328.

(9) Doorn, J. A., and Petersen, D. R. (2002) Covalent modification of amino acid nucleophiles by the lipid peroxidation products 4-hydroxy-2-nonenal and 4-oxo-2-nonenal. *Chem. Res. Toxicol. 15*, 1445–1450.

(10) Zhang, W. H., Liu, J., Xu, G., Yuan, Q., and Sayre, L. M. (2003) Model studies on protein side chain modification by 4-oxo-2-nonenal. *Chem. Res. Toxicol. 16*, 512–523.

(11) Sayre, L. M., Lin, D., Yuan, Q., Zhu, X., and Tang, X. (2006) Protein adducts generated from products of lipid oxidation: Focus on HNE and ONE. *Drug Metab. Rev. 38*, 651–675.

(12) Parola, M., Bellomo, G., Robino, G., Barrera, G., and Dianzani, M. U. (1999) 4-Hydroxynonenal as a biological signal: Molecular basis and pathophysiological implications. *Antioxid. Redox Signaling 1*, 255–284.

(13) Poli, G., and Schaur, R. J. (2000) 4-Hydroxynonenal in the pathomechanisms of oxidative stress. *IUBMB Life 50*, 315–321.

(14) Nakashima, I., Liu, W., Akhand, A. A., Takeda, K., Kawamoto, Y., Kato, M., and Suzuki, H. (2003) 4-hydroxynonenal triggers multistep signal transduction cascades for suppression of cellular functions. *Mol. Aspects Med. 24*, 231–238.

(15) West, J. D., Ji, C., Duncan, S. T., Amarnath, V., Schneider, C., Rizzo, C. J., Brash, A. R., and Marnett, L. J. (2004) Induction of apoptosis in colorectal carcinoma cells treated with 4-hydroxy-2-nonenal and structurally related aldehydic products of lipid peroxidation. *Chem. Res. Toxicol. 17*, 453–462.

(16) West, J. D., and Marnett, L. J. (2005) Alterations in gene expression induced by the lipid peroxidation product, 4-hydroxy-2-nonenal. *Chem. Res. Toxicol. 18*, 1642–1653.

(17) West, J. D., and Marnett, L. J. (2006) Endogenous reactive intermediates as modulators of cell signaling and cell death. *Chem. Res. Toxicol. 19*, 173–194.

(18) Dwivedi, S., Sharma, A., Patrick, B., Sharma, R., and Awasthi, Y. C. (2007) Role of 4-hydroxynonenal and its metabolites in signaling. *Redox Rep. 12*, 4–10.

(19) Sayre, L. M., Zelasko, D. A., Harris, P. L., Perry, G., Salomon, R. G., and Smith, M. A. (1997) 4-Hydroxynonenal-derived advanced lipid peroxidation end products are increased in Alzheimer's disease. *J. Neurochem. 68*, 2092–2097.

(20) Yoritaka, A., Hattori, N., Uchida, K., Tanaka, M., Stadtman, E. R., and Mizuno, Y. (1996) Immunohistochemical detection of 4-hydroxynonenal protein adducts in Parkinson disease. *Proc. Natl. Acad. Sci. U.S.A. 93*, 2696–2701.

(21) Napoli, C., D'Armiento, F. P., Mancini, F. P., Postiglione, A., Witztum, J. L., Palumbo, G., and Palinski, W. (1997) Fatty streak formation occurs in human fetal aortas and is greatly enhanced by maternal hypercholesterolemia. Intimal accumulation of low density lipoprotein and its oxidation precede monocyte recruitment into early atherosclerotic lesions. *J. Clin. Invest. 100*, 2680–2690.

(22) Yamagami, K., Yamamoto, Y., Kume, M., Ishikawa, Y., Yamaoka, Y., Hiai, H., and Toyokuni, S. (2000) Formation of 8-hydroxy-2′-deoxyguanosine and 4-hydroxy-2-nonenal-modified proteins in rat liver after ischemia-reperfusion: Distinct localization of the two oxidatively modified products. *Antioxid. Redox Signaling 2*, 127–136.

(23) Winter, C. K., Segall, H. J., and Haddon, W. F. (1986) Formation of cyclic adducts of deoxyguanosine with the aldehydes *trans*-4-hydroxy-2-hexenal and *trans*-4-hydroxy-2-nonenal *in vitro*. *Cancer Res. 46*, 5682–5686.

(24) Douki, T., Odin, F., Caillat, S., Favier, A., and Cadet, J. (2004) Predominance of the 1,N^2-propano-2′-deoxyguanosine adduct among 4-hydroxy-2-nonenal-induced DNA lesions. *Free Radical Biol. Med. 37*, 62–70.

(25) Kowalczyk, P., Ciesla, J. M., Komisarski, M., Kusmierek, J. T., and Tudek, B. (2004) Long-chain adducts of *trans*-4-hydroxy-2-nonenal to DNA bases cause recombination, base substitutions and frameshift mutations in M13 phage. *Mutat. Res. 550*, 33–48.

(26) Xing, D. X., Sun, L. X., Cukier, R. I., and Bu, Y. X. (2007) Theoretical prediction of the p53 gene mutagenic mechanism induced by trans-4-hydroxy-2-nonenal. *J. Phys. Chem. B 111*, 5362–5371.

(27) Yi, P., Zhan, D., Samokyszyn, V. M., Doerge, D. R., and Fu, P. P. (1997) Synthesis and ^{32}P-postlabeling/high-performance liquid chromatography separation of diastereomeric 1,N^2-(1,3-propano)-2′-

deoxyguanosine 3′-phosphate adducts formed from 4-hydroxy-2-nonenal. *Chem. Res. Toxicol. 10*, 1259–1265.
(28) Chung, F. L., Nath, R. G., Ocando, J., Nishikawa, A., and Zhang, L. (2000) Deoxyguanosine adducts of *t*-4-hydroxy-2-nonenal are endogenous DNA lesions in rodents and humans: Detection and potential sources. *Cancer Res. 60*, 1507–1511.
(29) Wacker, M., Schuler, D., Wanek, P., and Eder, E. (2000) Development of a ^{32}P-postlabeling method for the detection of 1,N^2-propanodeoxyguanosine adducts of *trans*-4-hydroxy-2-nonenal in vivo. *Chem. Res. Toxicol. 13*, 1165–1173.
(30) Wacker, M., Wanek, P., and Eder, E. (2001) Detection of 1,N^2-propanodeoxyguanosine adducts of *trans*-4-hydroxy-2-nonenal after gavage of *trans*-4-hydroxy-2-nonenal or induction of lipid peroxidation with carbon tetrachloride in F344 rats. *Chem.-Biol. Interact. 137*, 269–283.
(31) Chung, F. L., and Zhang, L. (2002) Deoxyguanosine adducts of *tert*-4-hydroxy-2-nonenal as markers of endogenous DNA lesions. *Methods Enzymol. 353*, 523–536.
(32) Liu, X., Lovell, M. A., and Lynn, B. C. (2006) Detection and quantification of endogenous cyclic DNA adducts derived from *trans*-4-hydroxy-2-nonenal in human brain tissue by isotope dilution capillary liquid chromatography nanoelectrospray tandem mass spectrometry. *Chem. Res. Toxicol. 19*, 710–718.
(33) Pan, J., Davis, W., Trushin, N., Amin, S., Nath, R. G., Salem, N., Jr., and and Chung, F. L. (2006) A solid-phase extraction/high-performance liquid chromatography-based ^{32}P-postlabeling method for detection of cyclic 1,N^2- propanodeoxyguanosine adducts derived from enals. *Anal. Biochem. 348*, 15–23.
(34) Wang, H., and Rizzo, C. J. (2001) Stereocontrolled syntheses of all four stereoisomeric 1, N^2-deoxyguanosine adducts of the lipid peroxidation product *trans*-4-hydroxynonenal. *Org. Lett. 3*, 3603–3605.
(35) Wang, H., Kozekov, I. D., Harris, T. M., and Rizzo, C. J. (2003) Site-specific synthesis and reactivity of oligonucleotides containing stereochemically defined 1,N^2-deoxyguanosine adducts of the lipid peroxidation product *trans*-4-hydroxynonenal. *J. Am. Chem. Soc. 125*, 5687–5700.
(36) Huang, H., Wang, H., Qi, N., Kozekova, A., Rizzo, C. J., and Stone, M. P. (2008) Rearrangement of the (6*S*,8*R*,11*S*) and (6*R*,8*S*,11*R*) exocyclic 1,N^2-deoxyguanosine adducts of *trans*-4-hydroxynonena l to N^2-deoxyguanosine cyclic hemiacetal adducts when placed complementary to cytosine in duplex DNA. *J. Am. Chem. Soc. 130*, 10898–10906.
(37) Riggins, J. N., Pratt, D. A., Voehler, M., Daniels, J. S., and Marnett, L. J. (2004) Kinetics and mechanism of the general-acid-catalyzed ring-closure of the malondialdehyde-DNA adduct, N^2 (3-oxo-1-propenyl)deoxyguanosine (N^2OPdG-), to 3-(2′-deoxy-β-D-erythro-pentofuranosyl)pyrimido[1,2-α]purin-10(3*H*)-one (M_1dG). *J. Am. Chem. Soc. 126*, 10571–10581.
(38) Riggins, J. N., Daniels, J. S., Rouzer, C. A., and Marnett, L. J. (2004) Kinetic and thermodynamic analysis of the hydrolytic ring-opening of the malondialdehyde-deoxyguanosine adduct, 3-(2′-deoxy-β-D-erythro-pentofuranosyl)-pyrimido[1,2-α]purin-10(3*H*)-one. *J. Am. Chem. Soc. 126*, 8237–8243.
(39) Sodum, R. S., and Chung, F. L. (1988) 1,N^2-ethenodeoxyguanosine as a potential marker for DNA adduct formation by *trans*-4-hydroxy-2-nonenal. *Cancer Res. 48*, 320–323.
(40) Sodum, R. S., and Chung, F. L. (1989) Structural characterization of adducts formed in the reaction of 2,3-epoxy-4-hydroxynonanal with deoxyguanosine. *Chem. Res. Toxicol. 2*, 23–28.
(41) Sodum, R. S., and Chung, F. L. (1991) Stereoselective formation of *in vitro* nucleic acid adducts by 2,3-epoxy-4-hydroxynonanal. *Cancer Res. 51*, 137–143.
(42) Chen, H. J., and Chung, F. L. (1994) Formation of etheno adducts in reactions of enals via autoxidation. *Chem. Res. Toxicol. 7*, 857–860.
(43) el Ghissassi, F., Barbin, A., Nair, J., and Bartsch, H. (1995) Formation of 1,N^6-ethenoadenine and 3,N^4-ethenocytosine by lipid peroxidation products and nucleic acid bases. *Chem. Res. Toxicol. 8*, 278–283.
(44) Benamira, M., and Marnett, L. J. (1992) The lipid peroxidation product 4-hydroxynonenal is a potent inducer of the SOS response. *Mutat. Res. 293*, 1–10.
(45) Esterbauer, H., Eckl, P., and Ortner, A. (1990) Possible mutagens derived from lipids and lipid precursors. *Mutat. Res. 238*, 223–233.
(46) Eckl, P. M., Ortner, A., and Esterbauer, H. (1993) Genotoxic properties of 4-hydroxyalkenals and analogous aldehydes. *Mutat. Res. 290*, 183–192.
(47) Karlhuber, G. M., Bauer, H. C., and Eckl, P. M. (1997) Cytotoxic and genotoxic effects of 4-hydroxynonenal in cerebral endothelial cells. *Mutat. Res. 381*, 209–216.
(48) Eckl, P. M. (2003) Genotoxicity of HNE. *Mol. Aspects Med. 24*, 161–165.
(49) Emerit, I., Khan, S. H., and Esterbauer, H. (1991) Hydroxynonenal, a component of clastogenic factors? *Free Radical Biol. Med. 10*, 371–377.
(50) Chung, F. L., Komninou, D., Zhang, L., Nath, R., Pan, J., Amin, S., and Richie, J. (2005) Glutathione depletion enhances the formation of endogenous cyclic DNA adducts derived from *t*-4-hydroxy-2-nonenal in rat liver. *Chem. Res. Toxicol. 18*, 24–27.
(51) Falletti, O., Cadet, J., Favier, A., and Douki, T. (2007) Trapping of 4-hydroxynonenal by glutathione efficiently prevents formation of DNA adducts in human cells. *Free Radical Biol. Med. 42*, 1258–1269.
(52) Yadav, U. C., Ramana, K. V., Awasthi, Y. C., and Srivastava, S. K. (2008) Glutathione level regulates HNE-induced genotoxicity in human erythroleukemia cells. *Toxicol. Appl. Pharmacol. 227*, 257–264.
(53) Cajelli, E., Ferraris, A., and Brambilla, G. (1987) Mutagenicity of 4-hydroxynonenal in V79 Chinese hamster cells. *Mutat. Res. 190*, 169–171.
(54) Chung, F. L., Chen, H. J., Guttenplan, J. B., Nishikawa, A., and Hard, G. C. (1993) 2,3-epoxy-4-hydroxynonanal as a potential tumor-initiating agent of lipid peroxidation. *Carcinogenesis 14*, 2073–2077.
(55) Hussain, S. P., Raja, K., Amstad, P. A., Sawyer, M., Trudel, L. J., Wogan, G. N., Hofseth, L. J., Shields, P. G., Billiar, T. R., Trautwein, C., Hohler, T., Galle, P. R., Phillips, D. H., Markin, R., Marrogi, A. J., and Harris, C. C. (2000) Increased p53 mutation load in nontumorous human liver of Wilson disease and hemochromatosis: Oxyradical overload diseases. *Proc. Natl. Acad. Sci. U.S.A. 97*, 12770–12775.
(56) Hu, W., Feng, Z., Eveleigh, J., Iyer, G., Pan, J., Amin, S., Chung, F. L., and Tang, M. S. (2002) The major lipid peroxidation product, *trans*-4-hydroxy-2-nonenal, preferentially forms DNA adducts at codon 249 of human p53 gene, a unique mutational hotspot in hepatocellular carcinoma. *Carcinogenesis 23*, 1781–1789.
(57) Feng, Z., Hu, W., Amin, S., and Tang, M. S. (2003) Mutational spectrum and genotoxicity of the major lipid peroxidation product, *trans*-4-hydroxy-2-nonenal, induced DNA adducts in nucleotide excision repair-proficient and -deficient human cells. *Biochemistry 42*, 7848–7854.
(58) Fernandes, P. H., Wang, H., Rizzo, C. J., and Lloyd, R. S. (2003) Site-specific mutagenicity of stereochemically defined 1,N^2-deoxyguanosine adducts of *trans*-4-hydroxynonenal in mammalian cells. *Environ. Mol. Mutagen. 42*, 68–74.
(59) Chung, F. L., Pan, J., Choudhury, S., Roy, R., Hu, W., and Tang, M. S. (2003) Formation of *trans*-4-hydroxy-2-nonenal- and other enal-derived cyclic DNA adducts from ω-3 and ω-6 polyunsaturated fatty acids and their roles in DNA repair and human p53 gene mutation. *Mutat. Res. 531*, 25–36.
(60) Choudhury, S., Pan, J., Amin, S., Chung, F. L., and Roy, R. (2004) Repair kinetics of *trans*-4-hydroxynonenal-induced cyclic 1,N^2-propanodeoxyguanine DNA adducts by human cell nuclear extracts. *Biochemistry 43*, 7514–7521.
(61) Wolfle, W. T., Johnson, R. E., Minko, I. G., Lloyd, R. S., Prakash, S., and Prakash, L. (2006) Replication past a trans-4-hydroxynonenal minor-groove adduct by the sequential action of human DNA polymerase l and k. *Mol. Cell. Biol. 26*, 381–386.
(62) Cavaluzzi, M. J., and Borer, P. N. (2004) Revised UV extinction coefficients for nucleoside-5′-monophosphates and unpaired DNA and RNA. *Nucleic Acids Res. 32*, e13.
(63) Piotto, M., Saudek, V., and Sklenar, V. (1992) Gradient-tailored excitation for single-quantum NMR spectroscopy of aqueous solutions. *J. Biomol. NMR 2*, 661–665.
(64) Sklenar, V., Bax, A., and Zon, G. (1986) Assignment of Z DNA NMR spectra of poly d(G^{m5}C) by two-dimensional multinuclear spectroscopy. *FEBS Lett. 208*, 94–98.
(65) Sklenar, V., Miyashiro, H., Zon, G., Miles, H. T., and Bax, A. (1986) Assignment of the ^{31}P and ^{1}H resonances in oligonucleotides by two-dimensional NMR spectroscopy. *FEBS Lett. 208*, 94–98.
(66) James, T. L. (1991) Relaxation matrix analysis of two-dimensional nuclear Overhauser effect spectra. *Curr. Opin. Struct. Biol. 1*, 1042–1053.
(67) Keepers, J. W., and James, T. L. (1984) A theoretical study of distance determinations from NMR—Two-dimensional nuclear Overhauser effect spectra. *J. Magn. Reson. 57*, 404–426.
(68) Borgias, B. A., and James, T. L. (1989) Two-dimensional nuclear Overhauser effect: Complete relaxation matrix analysis. *Methods Enzymol. 176*, 169–183.
(69) Borgias, B. A., and James, T. L. (1990) MARDIGRAS—A procedure for matrix analysis of relaxation for discerning geometry of an aqueous structure. *J. Magn. Reson. 87*, 475–487.
(70) Liu, H., Spielmann, H. P., Ulyanov, N. B., Wemmer, D. E., and James, T. L. (1995) Interproton distance bounds from 2D NOE intensities: Effect of experimental noise and peak integration errors. *J. Biomol. NMR 6*, 390–402.

(71) Salazar, M., Fedoroff, O. Y., Miller, J. M., Ribeiro, N. S., and Reid, B. R. (1993) The DNA strand in DNA:RNA hybrid duplexes is neither B-form nor A-form in solution. *Biochemistry 32*, 4207–4215.

(72) Wang, H., Zuiderweg, E. R. P., and Glick, G. D. (1995) Solution structure of a disulfide cross-linked DNA hairpin. *J. Am. Chem. Soc. 117*, 2981–2991.

(73) Geen, H., and Freeman, R. (1991) Band-selective radiofrequency pulses. *J. Magn. Reson. 93*, 93–141.

(74) Lankhorst, P. P., Haasnoot, A. G., Erkelens, C., and Altona, C. (1984) Carbon-13 NMR in conformational analysis of nucleic acid fragments. 3. The magnitude of torsional angle in d(TpA) from CCOP and HCOP NMR coupling constants. *Nucleic Acids Res. 12*, 5419–5428.

(75) Frisch, M. J., Trucks, G. W., Schlegel, H. B., Scuseria, G. E., Robb, M. A., Cheeseman, J. R., Montgomery, J. A., Vreven, T., Kudin, K. N., Burant, J. C., Millam, J. M., Iyengar, S. S., Tomasi, J., Barone, V., Mennucci, B., Cossi, M., Scalmani, G., Rega, N., Petersson, G. A., Nakatsuji, H., Hada, M., Ehara, M., Toyota, K., Fukuda, R., Hasegawa, J., Ishida, M., Nakajima, T., Honda, Y., Kitao, O., Nakai, H., Klene, M., Li, X., Knox, J. E., Hratchian, H. P., Cross, J. B., Adamo, C., Jaramillo, J., Gomperts, R., Stratmann, R. E., Yazyev, O., Austin, A. J., Cammi, R., Pomelli, C., Pomelli, J., Ochterski, W., Ayala, P. Y., Morokuma, K., Voth, G. A., Salvador, P., Dannenberg, J. J., Zakrzewska, V. G., Daniels, A. D., Farkas, O., Rabuck, A. D., Raghavachari, K., and Ortiz, J. V. (2004) *GAUSSIAN 03*, Gaussian, Inc., Wallingford, CT.

(76) Kouchakdjian, M., Marinelli, E., Gao, X., Johnson, F., Grollman, A., and Patel, D. (1989) NMR studies of exocyclic 1,N^2-propanodeoxyguanosine adducts (X) opposite purines in DNA duplexes: Protonated X(*syn*):A(*anti*) pairing (acidic pH) and X(*syn*):G(*anti*) pairing (neutral pH) at the lesion site. *Biochemistry 28*, 5647–5657.

(77) Arnott, S., and Hukins, D. W. L. (1972) Optimised parameters for A-DNA and B-DNA. *Biochem. Biophys. Res. Commun. 47*, 1504–1509.

(78) Case, D. A., Pearlman, D. A., Caldwell, J. W., Cheatham, T. E., III, Wang, J., Ross, W. S., Simmerling, C. L., Darden, T. A., Merz, K. M., Stanton, R. V., Cheng, A. L., Vincent, J. J., Crowley, M., Tsui, V., Gohlke, H., Radmer, R. J., Duan, Y., Pitera, J., Massova, I., Seibel, G. L., Singh, U. C., Weiner, P. K., and Kollman, P. A. (2002) *AMBER 8.0*, University of California, San Francisco, CA.

(79) Hawkins, G. D., Cramer, C. J., and Truhlar, D. G. (1995) Pairwise solute descreening of solute charges from a dielectric medium. *Chem. Phys. Lett. 246*, 122–129.

(80) Hawkins, G. D., Cramer, C. J., and Truhlar, D. G. (1996) Parametrized models of aqueous free energies of solvation based on pairwise descreening of solute atomic charges from a dielectric medium. *J. Phys. Chem. 100*, 19824–19839.

(81) Tsui, V., and Case, D. A. (2000) Theory and applications of the generalized Born solvation model in macromolecular simulations. *Biopolymers 56*, 275–291.

(82) Ryckaert, J.-P., Ciccotti, G., and Berendsen, H. J. C. (1977) Numerical integration of the cartesian equations of motion of a system with constraints: Molecular dynamics of n-alkanes. *J. Comp. Physiol. 23*, 327–341.

(83) Liu, Y., Zhao, D., Altman, R., and Jardetzky, O. (1992) A systematic comparison of three structure determination methods from NMR data: Dependence upon quality and quantity of data. *J. Biomol. NMR 2*, 373–388.

(84) Thomas, P. D., Basus, V. J., and James, T. L. (1991) Protein solution structure determination using distances from two-dimensional nuclear Overhauser effect experiments: Effect of approximations on the accuracy of derived structures. *Proc. Natl. Acad. Sci. U.S.A. 88*, 1237–1241.

(85) Lu, X. J., and Olson, W. K. (2003) 3DNA: A software package for the analysis, rebuilding and visualization of three-dimensional nucleic acid structures. *Nucleic Acids Res. 31*, 5108–5121.

(86) Patel, D. J., Shapiro, L., and Hare, D. (1987) DNA and RNA: NMR studies of conformations and dynamics in solution. *Q. Rev. Biophys. 20*, 35–112.

(87) Reid, B. R. (1987) Sequence-specific assignments and their use in NMR studies of DNA structure. *Q. Rev. Biophys. 20*, 2–28.

(88) Boelens, R., Scheek, R. M., Dijkstra, K., and Kaptein, R. (1985) Sequential assignment of imino- and amino-proton resonances in ^{1}H NMR spectra of oligonucleotides by two-dimensional NMR spectroscopy. Application to a*lac* operator fragment. *J. Magn. Reson. 62*, 378–386.

(89) Weisenseel, J. P., Reddy, G. R., Marnett, L. J., and Stone, M. P. (2002) Structure of an oligodeoxynucleotide containing a 1,N^2-propanodeoxyguanosine adduct positioned in a palindrome derived from the *Salmonella typhimurium hisD3052* gene: Hoogsteen pairing at pH 5.2. *Chem. Res. Toxicol. 15*, 127–139.

(90) Szekely, J., Rizzo, C. J., and Marnett, L. J. (2008) Chemical properties of oxopropenyl adducts of purine and pyrimidine nucleosides and their reactivity toward amino acid cross-link formation. *J. Am. Chem. Soc. 130*, 2195–2201.

(91) Norman, D., Abuaf, P., Hingerty, B. E., Live, D., Grunberger, D., Broyde, S., and Patel, D. J. (1989) NMR and computational characterization of the N-(deoxyguanosin-8-yl)aminofluorene adduct [(AF)G] opposite adenosine in DNA: (AF)G[syn]:A[anti]pair formation and its pH dependence. *Biochemistry 28*, 7462–7476.

(92) Mao, B., Cosman, M., Hingerty, B. E., Broyde, S., and Patel, D. J. (1995) Solution conformation of [AF]dG opposite a−1 deletion site in a DNA duplex: Intercalation of the covalently attached aminoflourene ring into the helix with base displacement of the C8-modified *syn* guanine into the major groove. *Biochemistry 34*, 6226–6238.

(93) Cosman, M., Hingerty, B., Geacintov, N. E., Broyde, S., and Patel, D. J. (1995) Structural alignments of (+)- and (-)-*trans-anti*-benzo[*a*]pyrene-dG adducts positioned at a DNA template/primer junction. *Biochemistry 34*, 15334–15350.

(94) Mao, B., Gorin, A., Gu, Z., Hingerty, B. E., Broyde, S., and Patel, D. J. (1997) Solution structure of the aminofluorene-intercalated conformer of the *syn* [AF]-C8-dG adduct opposite a−2 deletion site in the *Nar*I hot spot sequence context. *Biochemistry 36*, 14479–14490.

(95) Singh, U. S., Moe, J. G., Reddy, G. R., Weisenseel, J. P., Marnett, L. J., and Stone, M. P. (1993) ^{1}H NMR of an oligodeoxynucleotide containing a propanodeoxyguanosine adduct positioned in a $(CG)_3$ frameshift hotspot of *Salmonella typhimurium hisD3052*: Hoogsteen base-pairing at pH 5.8. *Chem. Res. Toxicol. 6*, 825–836.

(96) Kim, H. Y., Voehler, M., Harris, T. M., and Stone, M. P. (2002) Detection of an interchain carbinolamine cross-link formed in a CpG sequence by the acrolein DNA adduct γ-OH-1,N^2-propano-2′-deoxyguanosine. *J. Am. Chem. Soc. 124*, 9324–9325.

(97) Muth, G. W., Ortoleva-Donnelly, L., and Strobel, S. A. (2000) A single adenosine with a neutral pKa in the ribosomal peptidyl transferase center. *Science 289*, 947–950.

(98) de los Santos, C., Zaliznyak, T., and Johnson, F. (2001) NMR characterization of a DNA duplex containing the major acrolein-derived deoxyguanosine adduct γ-OH-1,N^2-propano-2′-deoxyguanosine. *J. Biol. Chem. 276*, 9077–9082.

(99) Stone, M. P., Cho, Y.-J., Huang, H., Kim, H.-Y., Kozekov, I. D., Kozekova, A., Wang, H., Lloyd, R. S., Harris, T. M., and Rizzo, C. J. (2008) Interstrand DNA cross-links induced by α,β-unsaturated aldehydes derived from lipid peroxidation and environmental sources. *Acc. Chem. Res. 41*, 793–804.

(100) Cho, Y. J., Wang, H., Kozekov, I. D., Kurtz, A. J., Jacob, J., Voehler, M., Smith, J., Harris, T. M., Lloyd, R. S., Rizzo, C. J., and Stone, M. P. (2006) Stereospecific formation of interstrand carbinolamine DNA cross-links by crotonaldehyde- and acetaldehyde-derived α-CH_3-γ-OH-1,N^2-propano-2′-deoxyguanosine adducts in the 5′-CpG-3′ sequence. *Chem. Res. Toxicol. 19*, 195–208.

(101) Kozekov, I. D., Nechev, L. V., Sanchez, A., Harris, C. M., Lloyd, R. S., and Harris, T. M. (2001) Interchain cross-linking of DNA mediated by the principal adduct of acrolein. *Chem. Res. Toxicol. 14*, 1482–1485.

(102) Kozekov, I. D., Nechev, L. V., Moseley, M. S., Harris, C. M., Rizzo, C. J., Stone, M. P., and Harris, T. M. (2003) DNA interchain cross-links formed by acrolein and crotonaldehyde. *J. Am. Chem. Soc. 125*, 50–61.

(103) Lao, Y., and Hecht, S. S. (2005) Synthesis and properties of an acetaldehyde-derived oligonucleotide interstrand cross-link. *Chem. Res. Toxicol. 18*, 711–721.

(104) Huang, H., Wang, H., Qi, N., Lloyd, R. S., Rizzo, C. J., and Stone, M. P. (2008) The stereochemistry of *trans*-4-hydroxynonenal-derived exocyclic 1,N^2-2′-deoxyguanosine adducts modulates formation of interstrand cross-links in the 5′-CpG-3′ sequence. *Biochemistry 47*, 11457–11472.

(105) VanderVeen, L. A., Hashim, M. F., Nechev, L. V., Harris, T. M., Harris, C. M., and Marnett, L. J. (2001) Evaluation of the mutagenic potential of the principal DNA adduct of acrolein. *J. Biol. Chem. 276*, 9066–9070.

(106) Yang, I. Y., Hossain, M., Miller, H., Khullar, S., Johnson, F., Grollman, A., and Moriya, M. (2001) Responses to the major acrolein-derived deoxyguanosine adduct in *Escherichia coli*. *J. Biol. Chem. 276*, 9071–9076.

(107) Fernandes, P. H., Kanuri, M., Nechev, L. V., Harris, T. M., and Lloyd, R. S. (2005) Mammalian cell mutagenesis of the DNA adducts of vinyl chloride and crotonaldehyde. *Environ. Mol. Mutagen. 45*, 455–459.

(108) Howell, C. A., Kondratick, C. M., and Washington, M. T. (2008) Substitution of a residue contacting the triphosphate moiety of the incoming nucleotide increases the fidelity of yeast DNA polymerase zeta. *Nucleic Acids Res. 36*, 1731–1740.

(109) Kouchakdjian, M., Eisenberg, M., Live, D., Marinelli, E., Grollman, A. P., and Patel, D. J. (1990) NMR studies of an exocyclic 1,N^2-propanodeoxyguanosine adduct (X) located opposite deoxyadenosine

(A) in DNA duplexes at basic pH: Simultaneous partial intercalation of X and A between stacked bases. *Biochemistry 29*, 4456–4465.

(110) Kouchakdjian, M., Eisenberg, M., Johnson, F., Grollman, A. P., and Patel, D. J. (1991) Structural features of an exocyclic adduct positioned opposite an abasic site in a DNA duplex. *Biochemistry 30*, 3262–3270.

(111) Huang, P., and Eisenberg, M. (1992) The three-dimensional structure in solution (pH 5.8) of a DNA 9-mer duplex containing 1,N^2-propanodeoxyguanosine opposite deoxyadenosine. Restrained molecular dynamics and NOE-based refinement calculations. *Biochemistry 31*, 6518–6532.

(112) Huang, P., Patel, D. J., and Eisenberg, M. (1993) Solution structure of the exocyclic 1,N^2-propanodeoxyguanosine adduct opposite deoxyadenosine in a DNA nonamer duplex at pH 8.9. Model of pH-dependent conformational transition. *Biochemistry 32*, 3852–3866.

(113) Moe, J. G., Reddy, G. R., Marnett, L. J., and Stone, M. P. (1994) ^{1}H NMR characterization of a duplex oligodeoxynucleotide containing propanodeoxyguanosine opposite a two-base deletion in the $(CpG)_3$ frameshift hotspot of *Salmonella typhimurium hisD3052*. *Chem. Res. Toxicol. 7*, 319–328.

(114) Weisenseel, J. P., Moe, J. G., Reddy, G. R., Marnett, L. J., and Stone, M. P. (1995) Structure of a duplex oligodeoxynucleotide containing propanodeoxyguanosine opposite a two-base deletion in the $(CpG)_3$ frameshift hotspot of *Salmonella typhimurium hisD3052* determined by ^{1}H NMR and restrained molecular dynamics. *Biochemistry 34*, 50–64.

(115) Weisenseel, J. P., Reddy, G. R., Marnett, L. J., and Stone, M. P. (2002) Structure of the 1,N^2-propanodeoxyguanosine adduct in a three-base DNA hairpin loop derived from a palindrome in the *Salmonella typhimurium hisD3052* gene. *Chem. Res. Toxicol. 15*, 140–152.

(116) Plum, G. E., Grollman, A. P., Johnson, F., and Breslauer, K. J. (1992) Influence of an exocyclic guanine adduct on the thermal stability, conformation, and melting thermodynamics of a DNA duplex. *Biochemistry 31*, 12096–12102.

(117) Shanmugam, G., Goodenough, A. K., Kozekov, I. D., Guengerich, F. P., Rizzo, C. J., and Stone, M. P. (2007) Structure of the 1,N^2-etheno-2′-deoxyguanosine adduct in duplex DNA at pH 8.6. *Chem. Res. Toxicol. 20*, 1601–1611.

(118) Zaliznyak, T., Lukin, M., Johnson, F., and de los Santos, C. (2008) Solution structure of duplex DNA containing the mutagenic lesion 1,N^2-etheno-2′-deoxyguanine. *Biochemistry 47*, 4606–4613.

(119) Shanmugam, G., Kozekov, I. D., Guengerich, F. P., Rizzo, C. J., and Stone, M. P. (2008) Structure of the 1N^2-ethenodeoxyguanosine adduct opposite cytosine in duplex DNA: Hoogsteen base pairing at pH 5.2. *Chem. Res. Toxicol. 21*, 1795–1805.

TX800320M